STRESS DISTRIBUTION IN MODELS SUBJECTED TO DYNAMIC LOADING

by

HERMAN CASPER SCHLAPPI

A THESIS

submitted to

OREGON STATE COLLEGE

in partial fulfillment of
the requirements for the
degree of

MASTER OF SCIENCE

June 1952

APPROVED:

Redacted for Privacy

Professor of Mechanical Engineering

In Charge of Major

Redacted for Privacy

Head of Department of Mechanical Engineering

Redacted for Privacy

Chairman of School Graduate Committee

Redacted for Privacy

Dean of Graduate School

Date thesis is presented June 1952

Typed by Jean Schlappi

TABLE OF CONTENTS

NOTATIONS

h	depth of beam	in.
t	thickness of beam	in.
L	length of beam	in.
L_e	effective length of beam	in.
A	th cross-sectional area	sq in.
ρ	density	$lb/in.^3$
E	modulus of elasticity	lb/sq in.
g	acceleration of gravity	$386\ in./sec^2$
t	time	sec
f	frequency	cycle/sec
$\omega = 2\pi f$	circular frequency	rad/sec
n	fringe order	
M	bending moment	lb in.
λ	wave length	Angstrom units
r	fillet radius	in.
x	distance measured along length of beam	in.
y	deflection	in.
y_m	maximum deflection	in.
p	maximum principal stress	lb/sq in.
q	minimum principal stress	lb/sq in.
σ	stress at outer fibers of beam	lb/sq in.
a	amplitude of vibration of testing machine table	in.

$$k = \left[\frac{\rho A \omega^2}{EIg}\right]^{\frac{1}{4}}$$ in.$^{-1}$

$I = \frac{th^3}{12}$ moment of inertia in.^{4}

$f = (P-q)\frac{t}{n}$ fringe constant lb/in./order

STRESS DISTRIBUTION IN MODELS SUBJECTED TO DYNAMIC LOADING

INTRODUCTION

The photoelastic method of stress analysis has won wide acceptance during recent years and at the present time ranks as one of the foremost tools in the field of experimental stress analysis. The increased use of the photoelastic and other experimental methods of stress analysis has been brought about by an increase in the number of problems which are too cumbersome or impossible to solve theoretically.

The dynamic stresses due to impact and vibration are of major concern in the design of present day structures and high speed machinery. The complex shape and loading, on many structures subjected to dynamic loading, have prevented theoretical analysis and experimental methods are required to determine the stress conditions.

Electrical resistance strain gages are widely used for determining dynamic stresses in full size prototypes. These gages measure the average strain over a finite gage length and are not well adapted for determining the stress distribution at points of high stress gradient, such as exist at discontinuities or points of high stress concentration.

In recent years considerable interest has been shown in the relatively new application of photoelasticity to the study of problems in dynamics. The stresses induced in models by impact, vibration and dynamic forces have been successfully determined photoelastically. Methods have also been developed for assessing transient stresses in photoelastic models.

The photoelastic method of analysis is relatively inexpensive and can be used to analyze problems which are difficult or impossible to solve by other methods. As better techniques and equipment are developed, an increased use of the photoelastic method can be expected in the analysis of dynamic problems.

This investigation was conducted to design, contruct and test a high speed polariscope suitable for the photoelastic analysis of dynamically loaded models. In preparation for this investigation a survey of the available literature on the subject was conducted to determine the present status of photoelasticity in the study of dynamics.

FUNDAMENTALS OF PHOTOELASTICITY

The photoelastic method of stress analysis is an experimental technique in which models cut from an appropriate transparent elastic material are tested. By applying the principles of similitude to the design of the model, the stress distribution in the prototype structure or machine element can be predicted. Loads are applied to the model in a manner similar to those existing on the prototype. When a stressed model is viewed in the polarized light of a polariscope, a series of dark and bright bands called interference fringes are observed. These fringes are an indication of the stress distribution in the model and through proper interpretation quantitative results can be obtained.

Many crystalline substances, such as calcite and tourmaline, have the property of resolving incident light into two components and transmitting it on planes which are orthogonal. Bakelite, a common photoelastic material, acquires this property of double refraction when subjected to stress.

The optical system employed for photoelastic studies is called a polariscope. The essential elements of the basic polariscope are a monochromatic light source, polarizer, analyzer and a camera or viewing screen for

observing or photographing the interference fringe patterns. The light first passes through the polarizer where it is plane polarized. As the emerging beam of polarized light enters the model, it is resolved into two components and transmitted along the planes of principle stress at each point in the model. Each component beam of polarized light is retarted an amount proportional to the principal stress whose direction is the same as the direction of polarization of the beam. In general, a phase difference between the two components will exist as they leave the model. This phase difference at any point is proportional to (p-q), the difference between the principal stresses at that point on the model. The analyzer measures this phase difference by bringing part of each component beam into interference in a single plane. The passage of light through all points of the model produces a continuous pattern consisting of light areas and dark interference fringes, which can be viewed visually or photographed.

The interference fringes representing a constant value of (p-q) are called isochromatics. Since the maximum shear stress at any point is equal to (p-q)/2, isochromatics can also be considered as the locus of points having the same maximum shearing stresses.

The relationship between (p-q) and the order of

interference is given by the equation

$$p-q = f\left(\frac{n}{t}\right)$$

where n is the order of interference, t the model thickness and f is the fringe constant or proportionality factor. The fringe constant is determined from a calibration test of a model which has an exact theoretical solution. (See Appendix I)

The directions of the principal stresses at all points of a model can also be determined photoelastically. The locus of points at which the principal directions are the same are called isoclinics and are indicated by a second set of interference fringes which are superimposed on the isochromatics.

The individual values of p and q at free boundaries can be determined photoelastically, since the stress normal to the boundary is zero. At interior points of the model additional data is required to determine the value of each principal stress.

From the theory of elasticity, it can be shown that the sum of the principal stresses (p+q) satisfy the Laplacian equation

$$\frac{\partial^2(p-q)}{\partial x^2} + \frac{\partial^2(p-q)}{\partial y^2} = 0$$

The numerical solution of this equation is a common method of determining (p+q), which combined with photoelastic values of (p-q) gives the principal stresses at all

interior points. Other methods of determining the interior values of the principal stresses are also available, however, they will not be discussed since they were not required for this investigation.

HISTORICAL BACKGROUND

The application of photoelasticity to dynamic problems is a fairly recent development and little experimental work has been done in the field. Since the literature on the subject is quite limited, the problems treated and the photoelastic methods employed by a few investigators will be briefly discussed.

In 1939 W. N. Findley (4, pp. 1-13) performed tests to determine the effect of high speed loading, acceleration of loading and the effect of body forces on the fundamental relations of photoelasticity as used for static work. A Bakelite beam was subjected to various rates of loading by a cam operating on a 25 inch flywheel. Stress patterns were photographed with a rotating camera. From these tests, the author concluded that the fringe constant for Bakelite is not dependent on loading rate, acceleration, or curvature, but is equal to the static value.

In 1936 Z. Tuzi and M. Nisida (15, pp. 448-473) made a photoelastic study of stresses due to impact. A continuous light source was used and a high speed film mounted on a rotating wheel was employed for taking pictures. A narrow slot placed in front of the rotating film was used to vary the exposure time. With a slot opening of 1/2 millimeter the 30 centimeter diameter

wheel rotating at 1400 revolutions per minute gave an exposure of 1/46,000 of a second. For exposure greater than 1/5,000 of a second a U-tube mercury arc lamp proved satisfactory, for shorter exposures illumination was insufficient and a standard carbon arc lamp with a deep red filter was used. Exposures of 1/50,000 of a second produced clear pictures with this light.

A swinging pendulum was used to subject a simply supported beam to an impact load at the center. The experimental values of the maximum dynamical stresses were found to be about 80 percent of the theoretical values. This difference was attributed to the absorbtion of energy which did not cause deflection. The results agreed more closely as L/b (the length to depth ratio) was increased.

A free falling weight was used to subject a cantilever beam model to an impact load at the free end. During the subsequent free lateral vibration of the beam, a continuous photographic record of the stress pattern at a section of the beam was obtained.

Three circular ring models of different geometric proportions were subjected to impact by a falling weight. The results obtained from the stress patterns approached the theoretical results more closely as R/b (the mean radius to width ratio) was increased. In all cases the

stresses obtained photoelastically were smaller than the theoretical values.

A photoelastic investigation of the stress conditions in a Bakelite beam vibrating at the fundamental resonant frequency was made by W. M. Murray (10, pp. 617-622) in 1941. A mercury stroboscope of the Edgerton type was used as a light source and a Wratten No. 62 filter was used to obtain a monochromatic band of light. Using a mechanical vibrator, resonant vibration at 3300 cycles per minute was induced in a cantilever beam 8 inches in length. A maximum deflection of 0.56 inches was produced at the free end of the cantilever beam. The results obtained from the stress patterns, photographed at a deflection of 0.44 inches, were in close agreement with the theoretical stresses at the outer fibers of the beam.

A method for measuring the transient stresses induced in photoelastic models was published by J. S. Stanton (11, p. 139) in 1949. A spark shadowgraph, like that used in the study of air waves, was employed. A critically damped spark which gave an exposure of the order of 1/10 of a microsecond was used as a light source. A time delay variable to alter the time of exposure was provided by a conventional multivibrator circuit.

A steel ball traveling at a velocity of 400 feet per second was fired against the end of a short plexiglas

cantilever beam protruding from a section of a larger size. Stress patterns were photographed for various time delays after impact. These patterns showed the propagation of the stress pattern in the model and the distribution of the transient stresses at short intervals after impact.

In 1941 F. S. Wyle (16, pp. 13-17) investigated the suitability of various light sources and filters for photoelastic studies in dynamics. The purpose of the investigation was to obtain (1) a stroboscope suitable for visual photoelastic examination of models with cyclic motion and (2) a high speed light for photographic recording of the stress patterns. A suitable high speed light source consisted of a standard Kadatron unit giving a light flash of 1/5,000 of a second duration and a No. 22 Wratten filter. When used with Verichrome film, nineteen orders of interference sharp enough for quantitative results were obtained. A Strobolux used with a No. 25 Wratten filter was found to be satisfactory for visual observation of models performing cyclic vibration.

A small portable polariscope suitable for photoelastic studies in dynamics was designed by J. J. Baruch (1, pp. 197-204) in 1950. A type 1532-A Stroboflash, which has a flash duration of approximately ten microseconds, was chosen as a light source for this instrument.

A Wratten No. 75 (eta) filter used in conjunction with commercial or process film was found to give a narrow band of monochromatic light peaked at 4800 Angstrom units. The band width was sufficiently narrow to obtain clear interference bands of order 20.

The stress patterns in a cantilever beam vibrating at 1710 cycles per minute was obtained using the above polariscope. Photographs of the transient fringe patterns induced in a cantilever beam by impact was also obtained.

THEORETICAL ANALYSIS

Lateral Vibration of Prismatic Beams

The differential equation for a beam subjected to a static uniform load of w pounds per unit length is

$$\frac{d^2}{dx^2}\left(EI\frac{d^2y}{dx^2}\right) = w \qquad (1)$$

where the deflection y is measured positive downwards. For beams of constant EI equation (1) reduces to

$$EI\frac{d^4y}{dx^4} = w. \qquad (2)$$

By applying D'Alembert's principle to the static equation (2), the equation for free lateral vibration is obtained. The inertia force acting per unit length along the beam is

$$-\frac{\rho A}{g}\frac{\partial^2 y}{\partial t^2}$$

where ρ is the density and A the cross-sectional area of the beam. Assuming that the inertia force is the only force acting and neglecting internal damping

$$EI\frac{\partial^4 y}{\partial x^4} = -\frac{\rho A}{g}\frac{\partial^2 y}{\partial t^2}$$

or

$$\frac{\partial^2 y}{\partial t^2} + a^2\frac{\partial^4 y}{\partial x^4} = 0 \qquad (3)$$

where $$a^2 = \frac{EIg}{\rho A} . \qquad (4)$$

During a normal mode of vibration the deflection at any point along the beam varies harmonically with time and can be represented by a function of the form

$$y = X (A \cos \omega t + B \sin \omega t) \qquad (5)$$

where X is a function of x determining the shape of the deflection curve. Substituting this value of y in equation (3)

$$\frac{d^4X}{dx^4} - K^4X = 0 \qquad (6)$$

where

$$K^4 = \frac{\omega^2 \rho A}{EIg} . \qquad (7)$$

The general solution of equation (6) is

$$X = C_1 \sin Kx + C_2 \cos Kx + C_3 \sinh Kx + C_4 \cosh Kx \qquad (8)$$

in which the four constants of integration are determined by the end conditions.

Substituting equation (8) in equation (5) the deflection curve for the fundamental mode of free lateral

vibration is

$$y = (C_1 \sin Kx + C_2 \cos Kx + C_3 \sinh Kx + C_4 \cosh Kx)(A \cos \omega t + B \sin \omega t). \quad (9)$$

Equation (9) contains seven constants: C_1 , C_2 , C_3 , C_4 , A, B, and ω , which depend upon the condition of support at the ends of the beam and the initial position of the beam at the time equal zero.

Lateral Vibration of a Cantilever Beam

It is advantageous to write the general solution, equation (8), in the form

$$X = C_1(\cos Kx + \cosh Kx) + C_2(\cos Kx - \cosh Kx) + C_3(\sin Kx + \sinh Kx) + C_4(\sin Kx - \sinh Kx) \quad (10)$$

when considering particular types of vibration.

Measuring the coordinate x from the free end of a cantilever beam, the end conditions are

(1) $X = 0$ at $x = L$

(2) $\frac{dX}{dx} = 0$ at $x = L$

(3) $\frac{d^2X}{dx^2} = 0$ at $x = 0$

(4) $\frac{d^3X}{dx^3} = 0$ at $x = 0$.

From conditions (3) and (4) $C_2 = C_4 = 0$ and from conditions (1) and (2) the following equations are obtained.

$$C_1(\cos KL + \cosh KL) + C_3(\sin KL + \sinh KL) = 0$$
$$-C_1(\sin KL + \sinh KL) + C_3(\cos KL + \cosh KL) = 0. \quad (11)$$

Equations (11) will have a solution other than $C_1 = C_3 = 0$ only if the determinate of the coefficients is zero. This condition yields the frequency equation

$$\cos KL \cosh KL = -1, \quad (12)$$

from which the natural frequencies of vibration are obtained. The first root of equation (12) corresponding to the fundamental mode of vibration is

$$KL = 1.875. \quad (13)$$

Setting $C_2 = C_4 = 0$ in equation (10) and substituting in equation (5) the deflection formula is

$$y = \left[C_1(\cos Kx + \cosh Kx) + C_3(\sin Kx + \sinh Kx)\right] \cdot (A \cos \omega t + B \sin \omega t). \quad (14)$$

Time will be measured from the position of zero deflection. This gives the initial condition, $y = 0$ when $t = 0$, at all points along the beam. Since C_1 and C_3 are not equal to zero,

$$A \cos \omega t + B \sin \omega t = 0$$

from which $A = 0$. Also, since $y = 0$ when $t = 0$ at all points, including $x = L$,

$$C_1(\cos KL + \cosh KL) + C_3(\sin KL + \sinh KL) = 0$$

or

$$C_3 = -0.734 C_1 \tag{15}$$

Substituting equation (15) in equation (12) and setting A = 0,

$$y = C\left[(\cos Kx + \cosh Kx) - 0.734 (\sin Kx + \sinh Kx)\right] \sin \omega t \tag{16}$$

where C is the combined constant C_1 B.

Let y_m be the maximum deflection at the free end of the beam during vibration. Then $y = y_m$ at $x = 0$ when $\omega t = \pi/2$. From these conditions $y_m = 2C$ or $C = \frac{1}{2} y_m$. Substituting the value C in equation (16) the deflection curve is given by the equation

$$y = \tfrac{1}{2} y_m \left[(\cos Kx + \cosh Kx) - 0.734 (\sin Kx + \sinh Kx)\right] \sin \omega t. \tag{17}$$

Differentiating equation (17) twice with respect to x

$$\frac{d^2y}{dx^2} = \tfrac{1}{2} K^2 y_m \left[(-\cos Kx + \cosh Kx) - 0.734 (-\sin Kx + \sinh Kx)\right] \sin \omega t. \tag{18}$$

The bending moment at any point x along the beam is

$$M = -EI \frac{d^2y}{dx^2} = \tfrac{1}{2} K^2 EI\, y_m \left[(\cos Kx - \cosh Kx) - 0.734(\sin Kx - \sinh Kx)\right] \sin \omega t. \tag{19}$$

The stress at the outer fibers at any point along the beam

is obtained from the equation

$$\sigma = \pm \frac{Mh}{2I}$$

from which

$$\sigma = \frac{1}{4} K^2 h E y_m \left[(\cos Kx - \cosh Kx) - 0.734 (\sin Kx - \sinh Kx) \right] \sin \omega t. \quad (20)$$

Substituting $K = 1.875 / L$ from equation (13)

$$\sigma = 0.878 E \left(\frac{h}{L^2}\right) y_m \left\{ \left[\cos 1.875\left(\frac{x}{L}\right) - \cosh 1.875\left(\frac{x}{L}\right) \right] - 0.734 \left[\sin 1.875\left(\frac{x}{L}\right) - \sinh 1.875\left(\frac{x}{L}\right) \right] \right\} \sin \omega t. \quad (21)$$

Lateral Vibration of a Pinned End Beam

The end conditions in the case of the simply supported or pinned end beam are

(1) $X = 0$ at $x = 0$

(2) $\frac{d^2X}{dx^2} = 0$ at $x = 0$

(3) $X = 0$ at $x = L$

(4) $\frac{d^2X}{dx^2} = 0$ at $x = L$

where L is the distance between the supports and the coordinate x is measured from the left support. From conditions (1) and (2) $C_1 = C_2 = 0$ in equation (10) and from conditions (3) and (4) the following equations are obtained.

$$C_3(\sin KL + \sinh KL) + C_4(\sin KL - \sinh KL) = 0$$
$$C_3(-\sin KL + \sinh KL) + C_4(-\sin KL - \sinh KL) = 0 \qquad (22)$$

Adding equation (22)

$$2C_3 \sinh KL - 2C_4 \sinh KL = 0$$

or

$$C_3 = C_4$$

Setting $C_1 = C_2 = 0$ and $C_3 = C_4$ in equation (10)

$$X = 2C_4 \sin Kx \qquad (23)$$

and the deflection equation is

$$y = 2C_4 \sin Kx (A \cos \omega t + B \sin \omega t) \qquad (24)$$

The frequency equation for the pinned end beam, obtained from equation (22) by setting the determinate of the coefficients equal to zero, is

$$\sin KL = 0 \qquad (25)$$

which has the roots $kL = \pi, 2\pi, 3\pi \ldots$. For the fundamental mode of vibration

$$KL = \pi \qquad (26)$$

Substituting $k = \pi/L$ in equation (24)

$$y = 2C_4 \sin \pi\left(\frac{x}{L}\right)\left(A \cos \omega t + B \sin \omega t\right) \qquad (27)$$

Measuring time from the undeflected position of the beam $y = 0$ when $t = 0$, therefore, $A = 0$ since C_4 is not zero and the deflection equation reduces to

$$y = C \sin \pi\left(\frac{x}{L}\right) \sin \omega t \qquad (28)$$

where C is the combined constant 2C B.

Let y_m be the maximum deflection at the center of the beam during vibration, then $y = y_m$ at $x = \frac{1}{2}$ when $\omega t = \pi/2$. Making these substitutions in equation (28)

$$C = y_m$$

and the deflection formula is

$$y = y_m \sin \pi\left(\frac{x}{L}\right) \sin \omega t . \qquad (29)$$

Differentiating equation (29) twice and substituting in the bending moment equation

$$M = EI\left(\frac{\pi}{L}\right)^2 y_m \sin \pi\left(\frac{x}{L}\right) \sin \omega t . \qquad (30)$$

The stress at the outer fibers of the beam is given by the equation

$$\sigma = \pm \frac{Mh}{2I}$$

from which

$$\sigma = \tfrac{1}{2} Eh\left(\frac{\pi}{L}\right)^2 y_m \sin \pi\left(\frac{x}{L}\right) \sin \omega t \qquad (31)$$

or

$$\sigma = 4.835 E\left(\frac{h}{L^2}\right) y_m \sin \pi\left(\frac{x}{L}\right) \sin \omega t . \qquad (32)$$

Natural Frequency and Effective Length of the Cantilever Beam

From equation (13), $kL = 1.875$, for the fundamental mode of vibration. Substituting

$$K = \left[\frac{\rho A \omega^2}{EIg}\right]^{\frac{1}{4}}$$

from equation (7),

$$\left[\frac{1.875}{L}\right]^{\frac{1}{4}} = \frac{\rho A \omega^2}{EIg} = \frac{12 \rho \omega^2}{E g h^2}$$

or

$$\omega = 1.017 \frac{h}{L^2} \sqrt{\frac{Eg}{\rho}} . \qquad (33)$$

Since $2\pi f = \omega$

$$f = 0.162 \frac{h}{L^2} \sqrt{\frac{Eg}{\rho}} . \qquad (34)$$

The period of vibration (the time required for one complete cycle) is $T = \frac{1}{f}$

or for the cantilever beam

$$T = 6.17 \frac{L^2}{h} \sqrt{\frac{\rho}{Eg}} . \qquad (35)$$

The effective length of a cantilever beam can be calculated from equation (34) if the lowest resonant frequency f is determined experimentally. The effective length L_e is usually slightly greater than the measured length because of the slight vibration of the clamped portion of the beam. From equation (34)

$$L^2 = 0.162 \frac{h}{f} \sqrt{\frac{Eg}{\rho}}$$

and the effective length is

$$L_e = 0.402 \left[\frac{Eg}{\rho}\right]^{\frac{1}{4}} \sqrt{\frac{h}{f}} . \qquad (36)$$

Natural Frequency and Effective Length of the Pinned End Beam

From equation (26) $kL = \pi$ for the fundamental mode of vibration of a pinned end beam. Substituting the value of k from equation (7)

$$k^4 = \frac{\pi^4}{L^4} = \frac{12\rho\omega^2}{Eg\,h^2}$$

from which

$$\omega = 2.86\,\frac{h}{L^2}\sqrt{\frac{Eg}{\rho}} \qquad (37)$$

and

$$f = 0.454\,\frac{h}{L^2}\sqrt{\frac{Eg}{\rho}}\,. \qquad (38)$$

The period of the pinned end beam is

$$T = \frac{1}{f} = 2.2\,\frac{L^2}{h}\sqrt{\frac{\rho}{Eg}}\,. \qquad (39)$$

The effective length of the pinned end beam is, from equation (38)

$$L_e = 0.675\left[\frac{Eg}{\rho}\right]^{\frac{1}{4}}\sqrt{\frac{h}{f}} \qquad (40)$$

where f is the lowest resonant frequency determined experimentally.

DEVELOPMENT OF TEST EQUIPMENT

A continuous light source of relatively low intensity is commonly used for photographing static stress patterns. Such a light is not satisfactory for dynamic studies, since the exposure time must be exceedingly short to obtain clear photographs of rapidly changing dynamic stress patterns. A light of extremely high intensity is required to fully expose the film during the short time of exposure. A short exposure time can be obtained by (1) using a single intense flash of short duration or (2) using a continuous light source of high intensity in conjunction with an extremely fast camera. The first method was employed in this investigation, since it requires less elaborate equipment and produces a polariscope which is suitable for both static and dynamic studies.

Light Source

A Type 1532-A Strobolume, manufactured by the General Radio Company, was chosen as a light source for the polariscope designed in this investigation. The Strobolume can be used to produce single flashes or as a stroboscopic intrument for short periods at repetition rates up to 1200 flashes per minute. The intensity of the light is approximately 8.5 million beam candlepower

and the duration of the flash of 40 microseconds. For single flash operation the light is flashed by a contactor in the low voltage triggering circuit. This contactor can be operated manually or by a mechanism designed to synchronize the flash with a presribed motion or event. The Strobolume can be triggered by a Type 631-BL or Type 631-B Strobotac for stroboscopic operation. When used in this manner, the lamps of both instruments flash simultaneously and the frequency of both is controlled by the Strobotac.

A Type 631-B Strobotac was used for stroboscopic operation of the Strobolume during this investigation. A push button switch placed in the triggering circuit allowed the power supply for the Strobolume to remain on continuously while permitting operation of the lamp only when required. The instruments employed as a light source are shown in Figure 1.

Polariscope

The polariscope was designed primarily for studying the stress conditions in models subjected to forced cyclic vibration. For this reason, the frame of the polariscope was constructed for mounting on a Model 10VA All American Vibration Fatigue Testing Machine, which was used to induce vibration in the photoelastic models. Four Lord shock mounts were used to isolate the polariscope from

Figure 1. Type 1532-A Strobolume and Type 631-B Strobotac.

the vibration of the machine base. The Strobolume lamp, Polaroids, filter and camera were mounted in an inverted position on overhead rails. These rails permitted longitudinal adjustment of the various elements. Two cross rails allowed lateral adjustment of the complete assembly. This arrangement was necessary to permit observation of the stress patterns throughout the entire length of the long beam models. Provisions were also provided for vertical adjustment of the polariscope.

The polarizer, quarter wave plates and analyzer from a conventional circular polariscope were used. The arrangement of these elements is shown in Figure 2.

A camera with a f/4.5 lens and a ground glass focus suitable for visual observation of stress patterns was

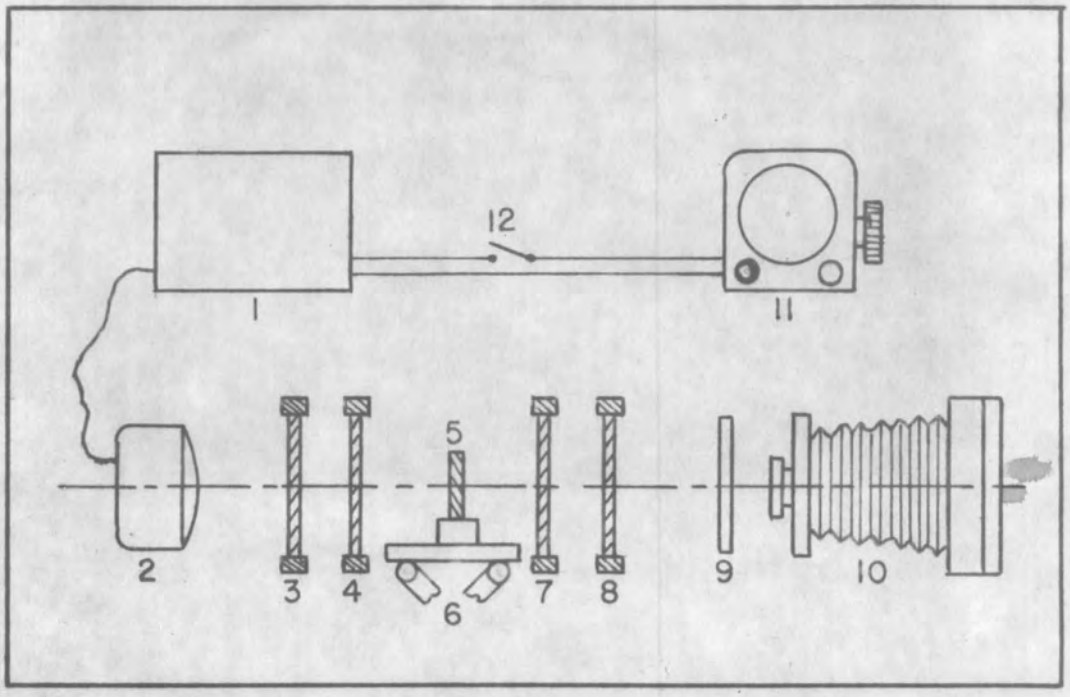

1. Type 1532-A Strobolume.
2. Strobolume lamp.
3. Polarizer.
4. Quarter wave plate.
5. Photoelastic model.
6. Table of Vibration Fatigue Testing Machine.
7. Quarter wave plate.
8. Analyzer.
9. Wratten No. 75 filter (six inches square).
10. Camera, f/4.5 lens, ground glass focus.
11. Type 631-B Strobotac.
12. Manual switch in triggering circuit.

Figure 2. Schematic diagram of polariscope and wiring connections between instruments.

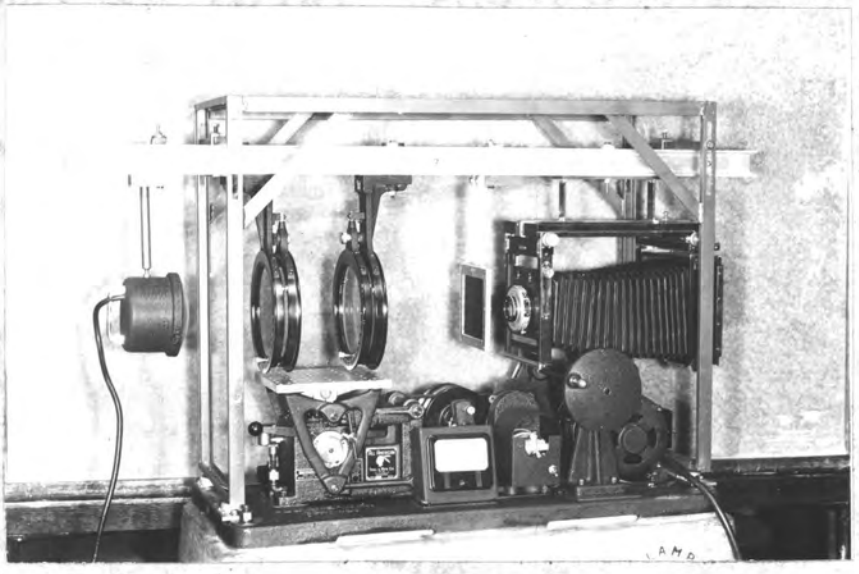

Figure 3. Front view of All American Vibration Fatigue Testing Machine with the high speed polariscope bolted in place.

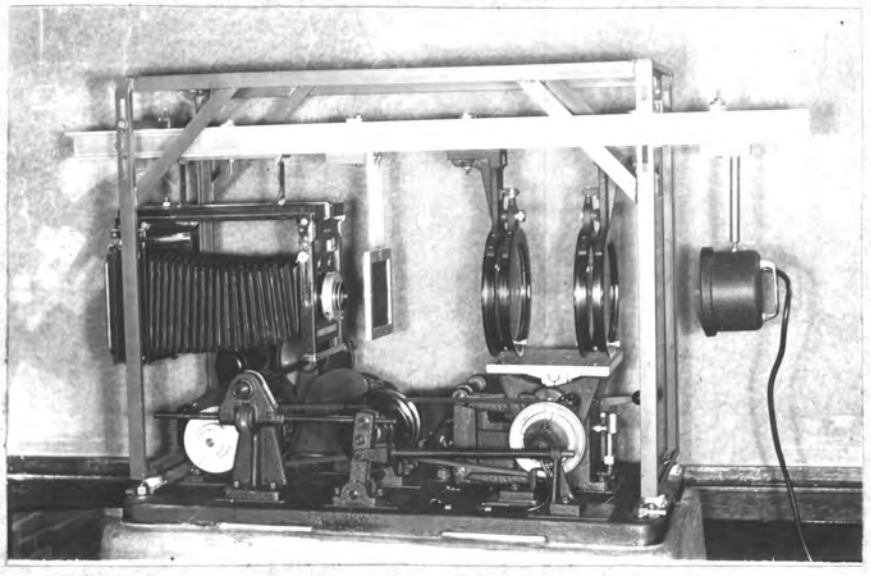

Figure 4. Rear view of All American Vibration Fatigue Testing Machine and high speed polariscope.

mounted as shown in Figures 3 and 4. A Wratten No. 75 filter was placed directly in front of the camera lens, which permitted the taking of photographs in a lighted room without fogging the film.

The filter-film combination used by J. J. Baruch (1, pp. 197-204) in designing a high speed polariscope was adopted for this polariscope. The Wratten No. 75 filter passes only a narrow band of blue-green light. When used with commercial film, which is highly sensitive to blue light, a very narrow band of blue-green monochromatic light is obtained. The Strobolume lamp, Wratten No. 75 filter and commercial film all have peaks at approximately 4800 Angstrom units and when the three are used together the resultant band width is only 2200 Angstrom units wide. With this arrangement, J. J. Baruch obtained clear stress patterns of order 20.

A diffuser was not used in this polariscope. As a result, the photoelastic field which could be illuminated was approximately 3 1/2 inches in diameter. The field size could have been increased to the full diameter of the Polaroids (approximately six inches) by placing a diffuser between the light source and the polarizer, however, this would have reduced the light intensity by a factor of four.

Preliminary tests of the polariscope indicated that

a single flash of 40 microseconds duration was sufficient to obtain good exposure using commercial film and models cut from S-4 48306 Bakelite.

Vibration Fatigue Testing Machine

A Model 10 VA All American Vibration Fatigue Testing Machine was used to induce vibration in the photoelastic models. This machine, with the complete polariscope mounted, is shown in Figures 3 and 4. The machine has a mechanically vibrated table capable of carrying loads up to 10 pounds in weight. A variable speed V-belt drive provides a continuous frequency range from 10 to 60 cycles per second and the amplitude of vibration of the table can be varied from zero to 0.2 inches. The table performs vertical harmonic motion which is ideally suited for inducing cyclic vibration in photoelastic models.

PHOTOELASTIC MODELS

Properties of S-4 48306 Bakelite

The photoelastic material used in this investigation was S-4 48306 Bakelite. This material has a high creep rate which limits its use for static models, however, it was felt that for vibrating models, where a complete reversal of stresses is occurring, this property would not be detrimental. Investigations by J. J. Baruch (1, p. 201) indicated that yellow Bakelites cause high attenuation of the 4800 Angstrom unit band of light, making a longer exposure necessary. Water clear S-4 48306 Bakelite does not cause this attenuation, a property which favored its use.

The fringe constant for S-4 48306 Bakelite was determined from a calibration test of a beam in pure bending. A value of 83.4 pounds per square inch per order of interference was obtained using the 4800 Angstrom unit band of light as a light source. This value was determined from a static test, however, W. M. Findley (4, P. 13) concluded from tests that the static and dynamic values of the fringe constant are equal. Details of the calibration test are given in Appendix I.

The modulus of elasticity of S-4 48306 Bakelite determined from a tension test of two specimens was 550,000 pounds per square inch. The stress patterns photographed during the calibration test indicated that the modulus of

elasticity was approximately the same in tension and compression. A stress-strain diagram for S-4 48306 Bakelite is included in Appendix II.

Construction of Models and Mounting Fixtures

Four photoelastic models, two cantilever beams and two pinned end beams, were tested in this investigation. The models were milled from sheets of polished S-4 48306 Bakelite approximately 3/8 of an inch in thickness. The dimensions of the cantilever and pinned end beams are given in the table of Figures 5 and 6. The fillet radius of Model No. 2 was decreased by increments to enable a study of the stress concentration at the fillet. It was also necessary to decrease the depth of Model No. 2 between tests to eliminate the edge effects of time.

The fixtures for mounting the models on the table of the testing machine are shown in Figures 7 and 8. The cantilever beam models were rigidly clamped with four bolts. A scale mounted at the end of the beam was used for measuring the deflection during vibration. The deflection of the pinned end beams was measured with a scale placed midway between the pin supports.

Lines were drawn with black ink at intervals of one inch throughout the length of the models. These lines aided in matching the various sections of the stress patterns and simplified the analysis.

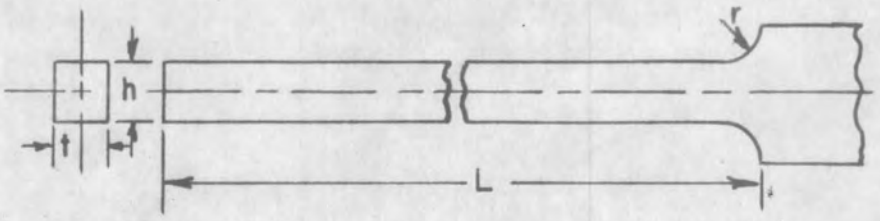

f = theoretical natural frequency in cycle/ sec.

MODEL NO.	r	t	h	L	f
	in.	in.	in.	in.	cps
1	1/4	0.340	0.375	9	50.5
2	3/8	0.317	0.430	10	46.8
	1/4	0.317	0.404	10	44.0
	1/8	0.317	0.375	10	40.8
	0	0.317	0.375	10	40.8

FIGURE 5. DIMENSIONS AND THEORETICAL NATURAL FREQUENCY OF CANTILEVER BEAMS.

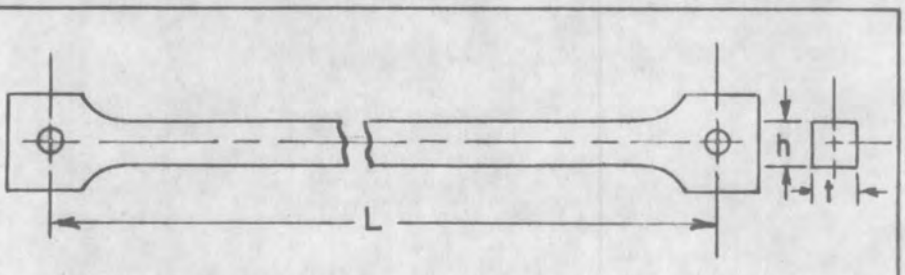

MODEL NO.	L	h	t	f
	in.	in.	in.	cps
3	11.75	0.250	0.327	55.2
4	12	0.275	0.325	58.2

FIGURE 6. DIMENSIONS AND THEORETICAL NATURAL FREQUENCY OF PINNED END BEAM MODELS.

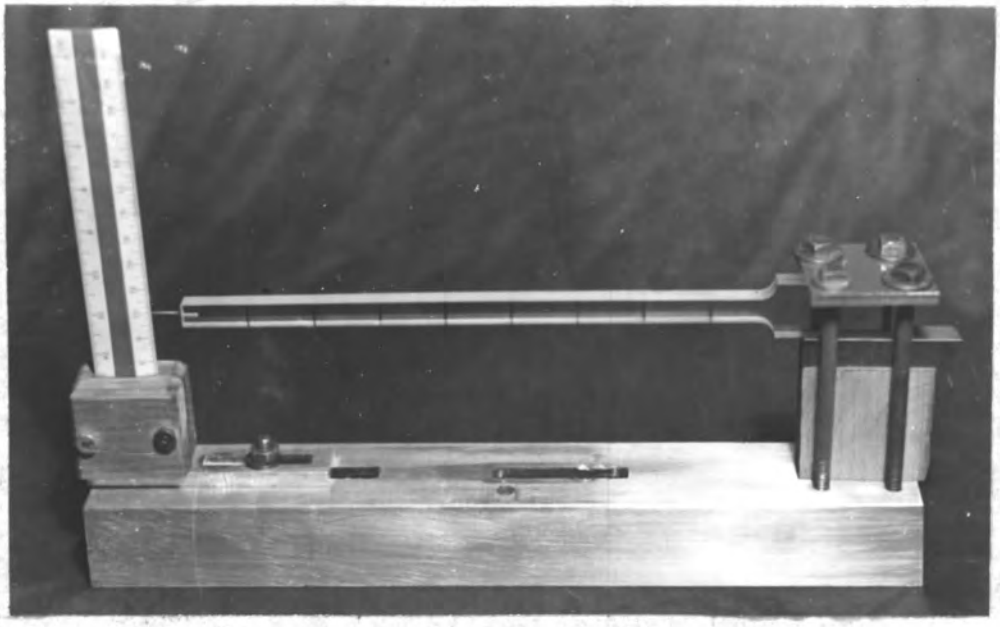

Figure 7. Cantilever beam assembly showing scale at free end for measuring deflection and the method of support at clamped end.

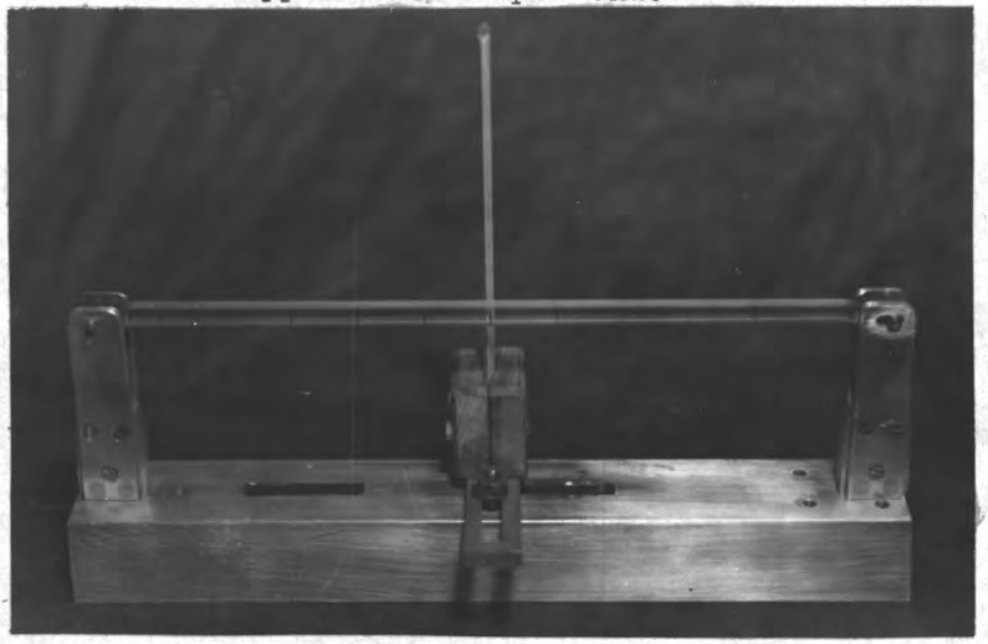

Figure 8. Pinned end beam assembly showing pin supports and position of scale for measuring deflection at center of beam.

TEST PROCEDURE

The cantilever beam assembly of Figure 7 is shown mounted on the table of the Vibration Fatigue Testing Machine in Figure 9.

The maximum deflection, produced in the models by vibration at the resonant frequency, was controlled by varying the amplitude of the table vibration. A few trials indicated that the maximum deflection induced in the models was proportional to the amplitude of vibration of the table. Thus, to double the deflection of a model the table amplitude was doubled.

The frequency at which resonance occurred in each model was easily recognized by the resulting large increase in deflection.

The stress patterns were observed visually and photographed using the Strobolume as a stroboscopic light source operated by a Type 631-B Strobotac. The stroboscopic light from the Strobotac was focused directly on the model to facilitate reading of the deflection and synchronization of the flashes with the motion of the beam. In order to keep the flashing rate below the maximum rate of the Strobolume (1200 flashes per minute), it was necessary to operate the Strobotac at a submultple of the beam frequency.

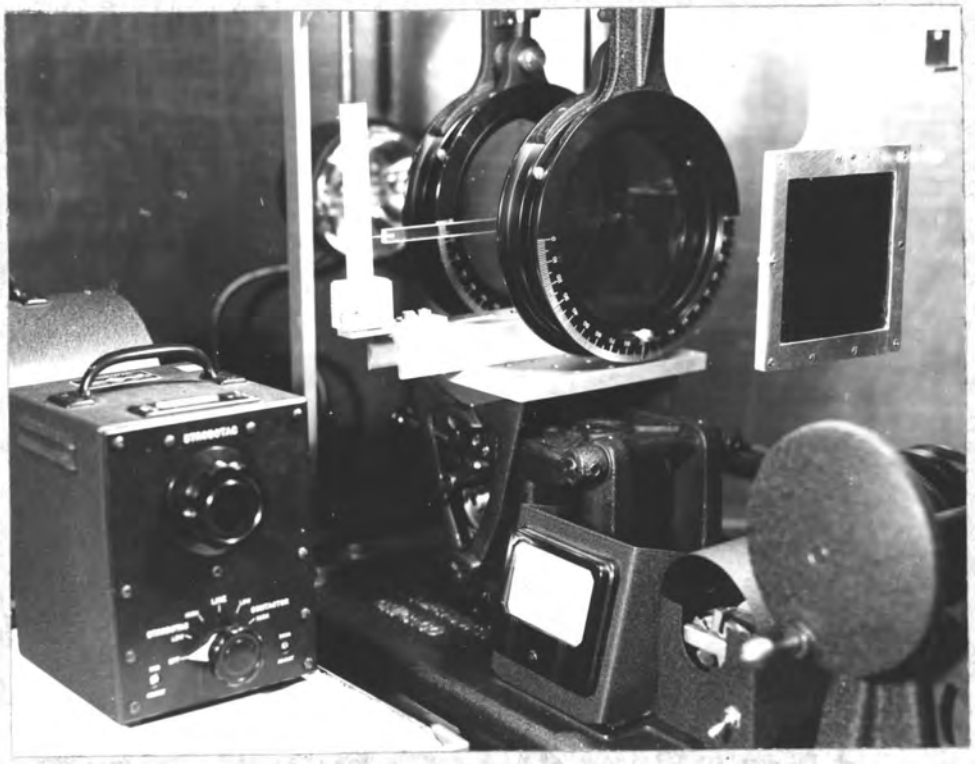

Figure 9. Cantilever beam assembly mounted in the polariscope on the table of the Vibration Fatigue Testing Machine.

Slight variations in the speed of the tesing machine made it difficult to view the beam in the same position for any great length of time. Fortunately, the cyclic change of the stress pattern, when viewed with the stroboscopic light source, was sufficiently slow to permit photographing of the stress patterns. The maximum deflection and the deflection at the instant the stress patterns were photographed was read to the nearest 1/100 of an inch directly from the scale.

The stress patterns were photographed at a shutter

speed of 1/5 of a second. Since the Strobolume was allowed to flash continuously, while taking a photograph, an exposure of 2 or 3 flashes was obtained during the time the shutter remained open.

Visual observation of stress patterns indicated that the first few flashes from the Strobolume were not synchronized with the Strobotac. Pictures taken during this period were blurred and showed stress patterns for several positions of the beam. For this reason, the Strobolume was allowed to flash several times before the camera shutter was opened.

The complete stress pattern of the long beam models could not be obtained with a single photograph and it was necessary to take photographs at several positions along the beam. This was accomplished by sliding the complete polariscope to different positions along the beam without stopping the testing machine or disturbing the vibration of the model. The photographs taken in the manner were found to match quite well, when photographed at the same deflection.

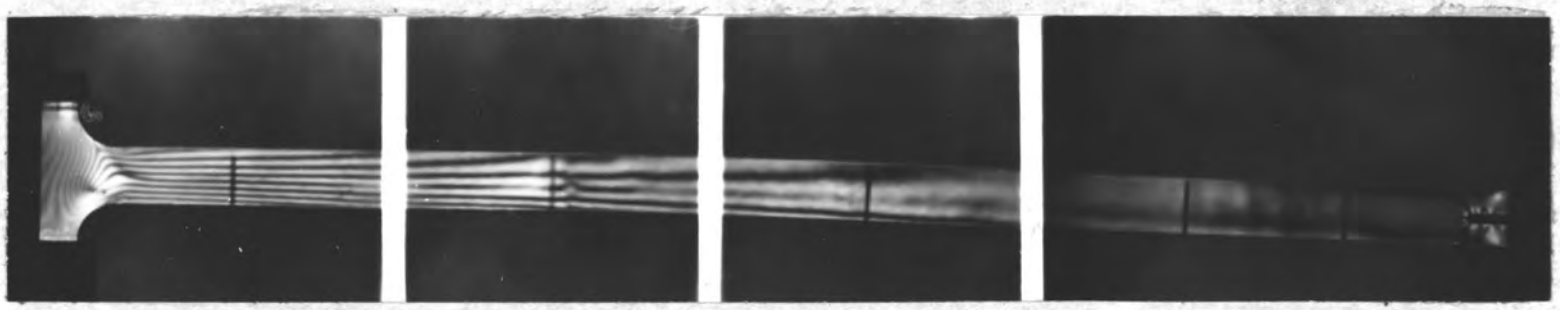

Figure 10. Stress patterns of a cantilever beam (Model No. 1) vibrating at the fundamental resonant frequency photographed at the time of maximum deflection. $y_m = 0.25$ in., $f = 55$ cycle/sec.

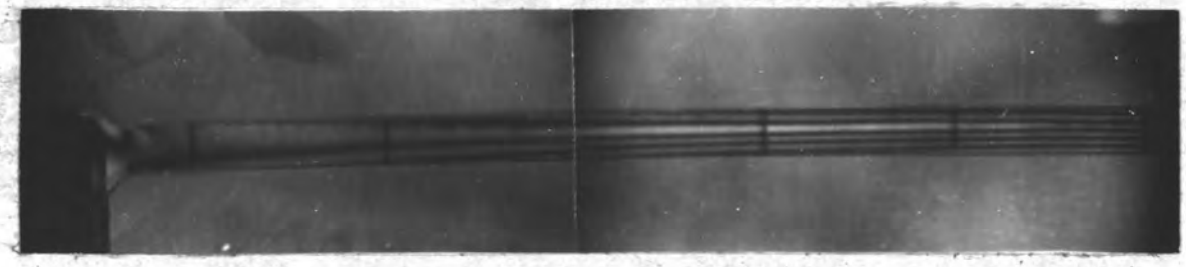

Figure 11. Stress patterns of a pinned end beam (Model No. 3) photographed at the time of maximum deflection during vibration at the lowest resonant frequency. $y_m = 0.14$ in., $f = 57.5$ cycle/sec.

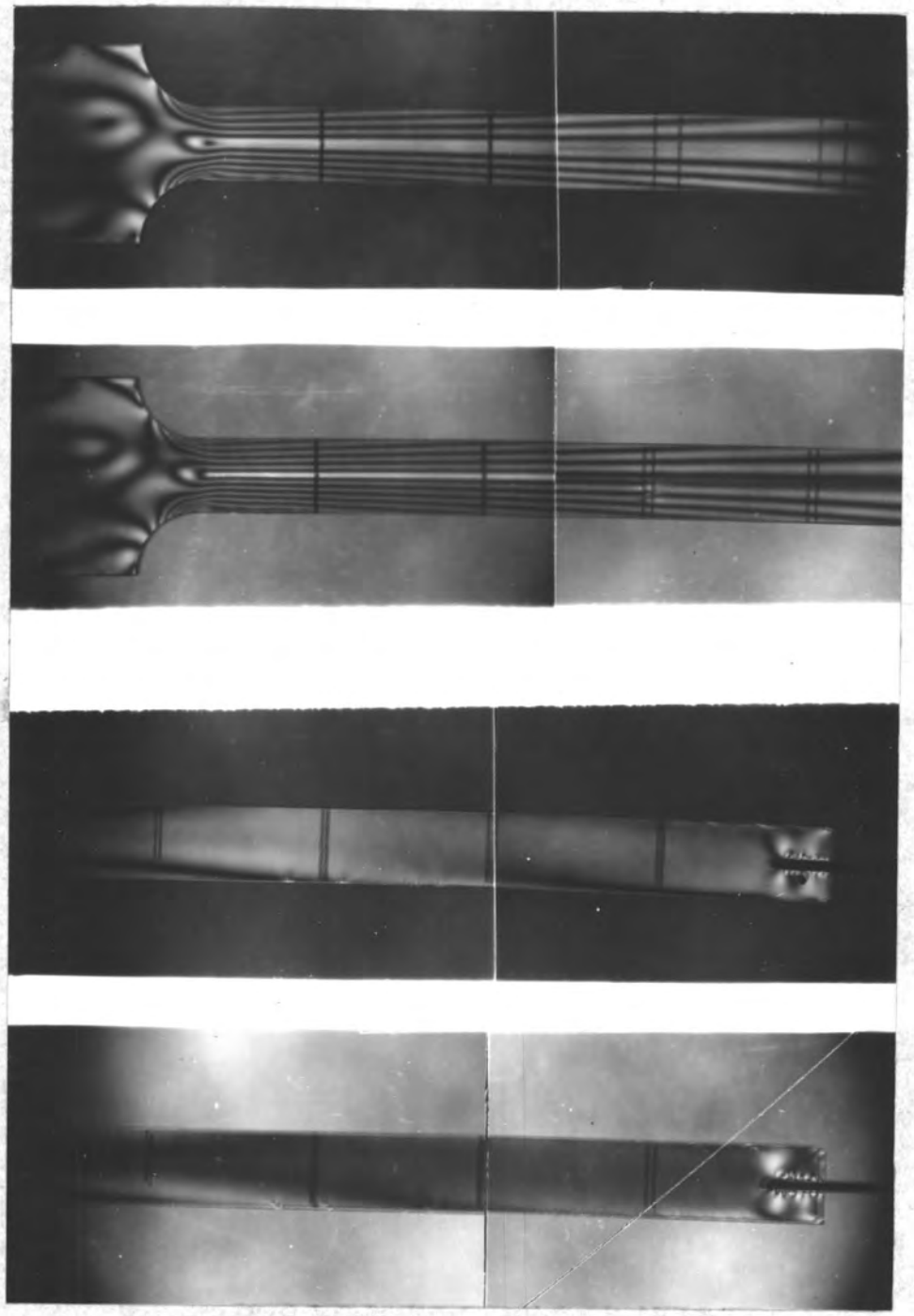

Figure 12. Stress patterns of a cantilever beam (Model No. 2) vibrating at the fundamental resonant frequency photographed at the point of maximum deflection. $y_m = 0.30$ in., $f = 50$ cycles/sec.

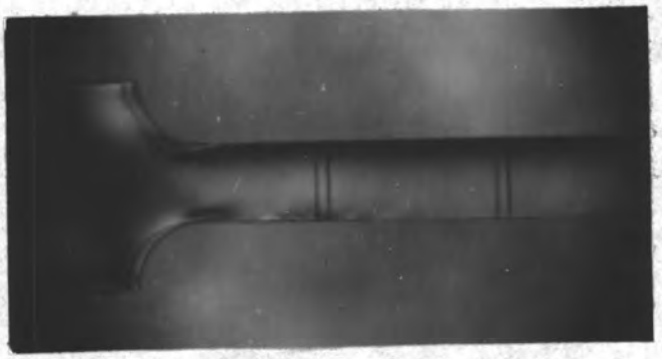

(a) $y = 0$, $t = 0$

(b) $y = 0.05$ in., $t = 0.00031$ sec

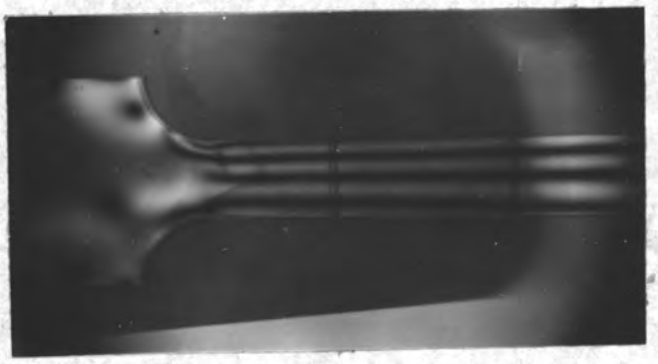

(c) $y = 0.10$ in., $t = 0.00062$ sec

Figure 13. Stress patterns at the clamped end of a cantilever beam (Model No. 2) at various deflections during resonant vibration at the fundamental natural frequency. $y_m = 0.52$ in. $f = 50$ cycle/sec.

(d) y = 0.20 in., t = 0.00126 sec

(e) y = 0.30 in., t = 0.00196 sec

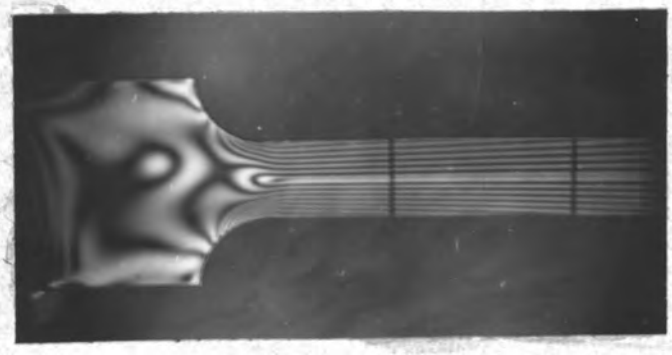

(f) y = 0.40 in., t = 0.00281 sec

Figure 14. Stress patterns at the clamped end of a cantilever beam (Model No. 2) at various deflections during resonant vibration at the fundamental natural frequency. y_m = 0.52 in., f = 50 cycle/sec.

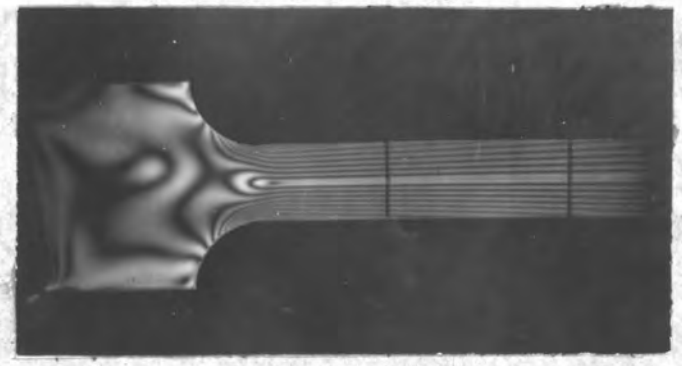

(g) $y = 0.45$ in., $t = 0.00334$ sec.

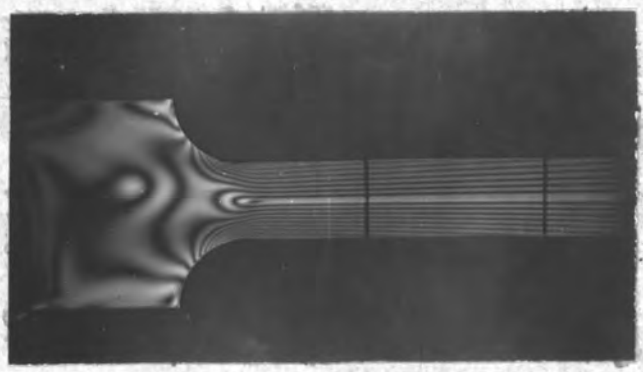

(h) $y = 0.52$ in., $t = 0.00502$ sec.

Figure 15. Stress patterns at the clamped end of a cantilever beam (Model No. 2) at various deflections during resonant vibration at the fundamental natural frequency. $y_m = 0.52$ in., $f = 50$ cycle/sec.

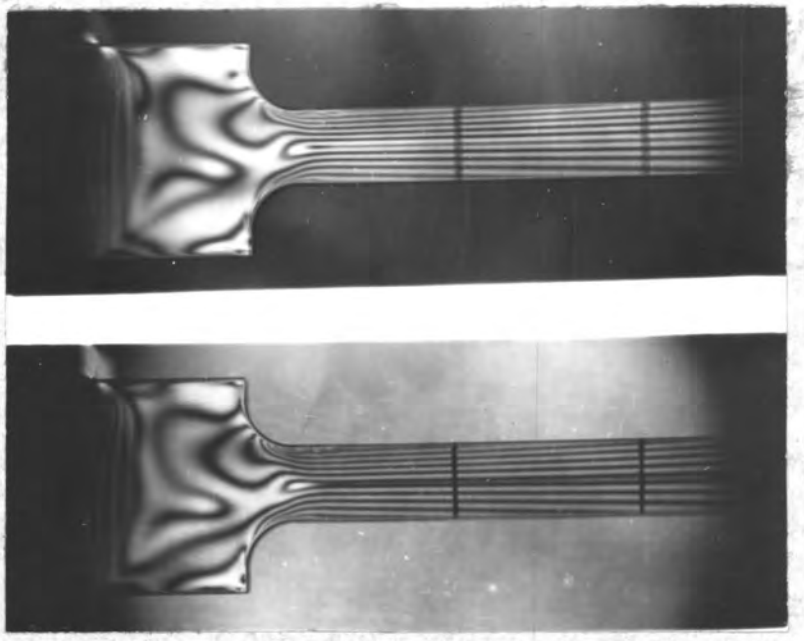

Figure 16. Stress patterns of a cantilever beam (Model No. 2) photographed at the point of maximum deflection during resonant vibration at the fundamental natural frequency. $y_m = 0.40$ in., $f = 46$ cycle/sec, $r = 1/4$ in.

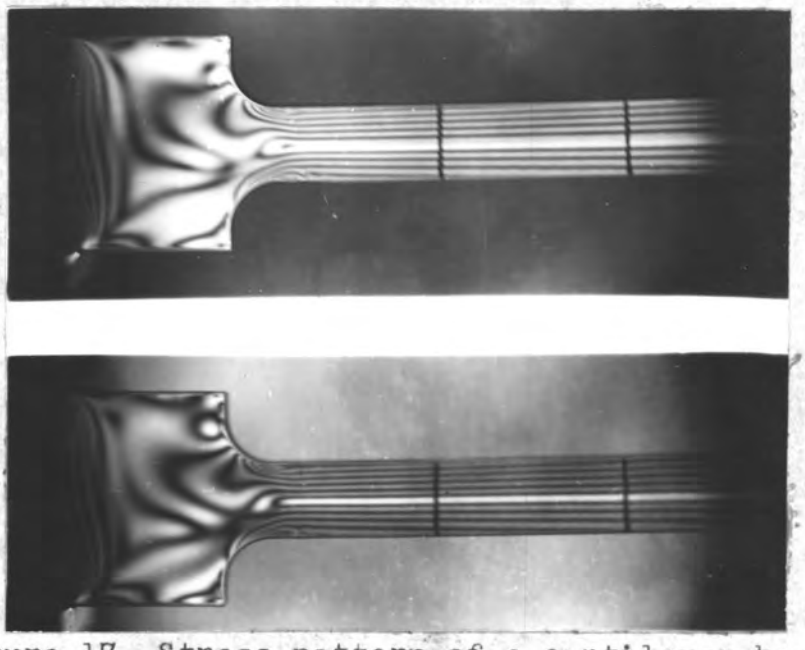

Figure 17. Stress pattern of a cantilever beam (Model No. 2) statically deflected by a concentrated load at the free end. $y = 0.40$ in., $r = 1/4$ in.

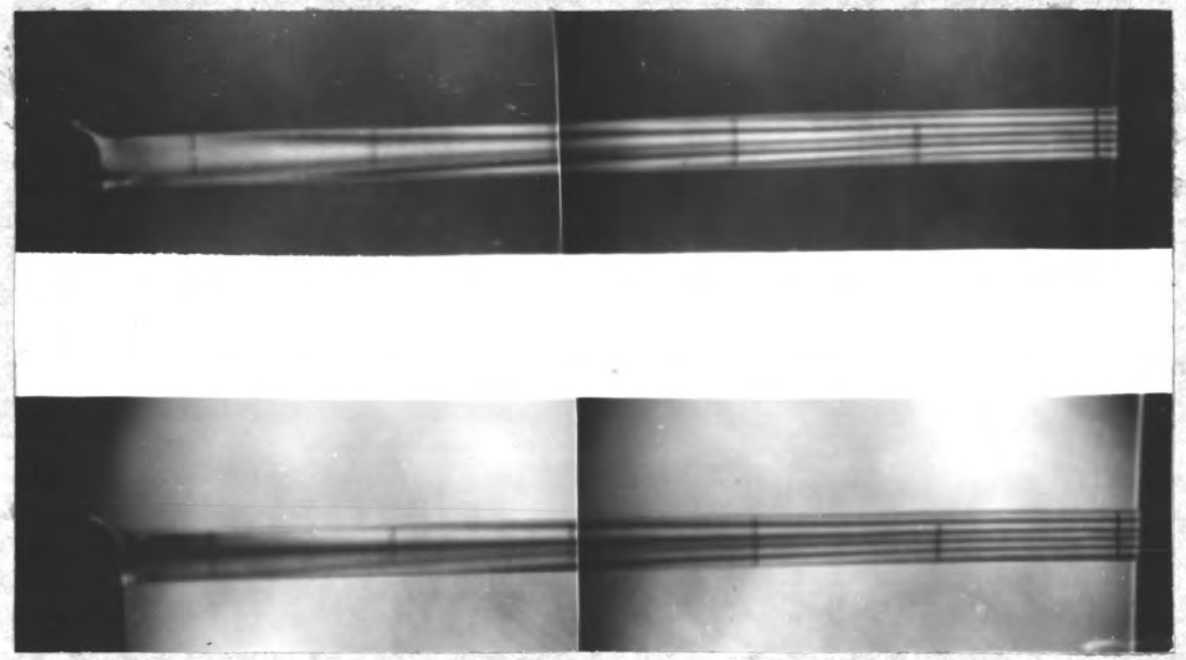

Figure 18. Stress patterns of a pinned end beam (Model No. 4) vibrating at the lowest resonant frequency photographed at the point of maximum deflection. $y_m = 0.12$ in., $f = 62$ cycle/sec, $a = 0.10$ in.

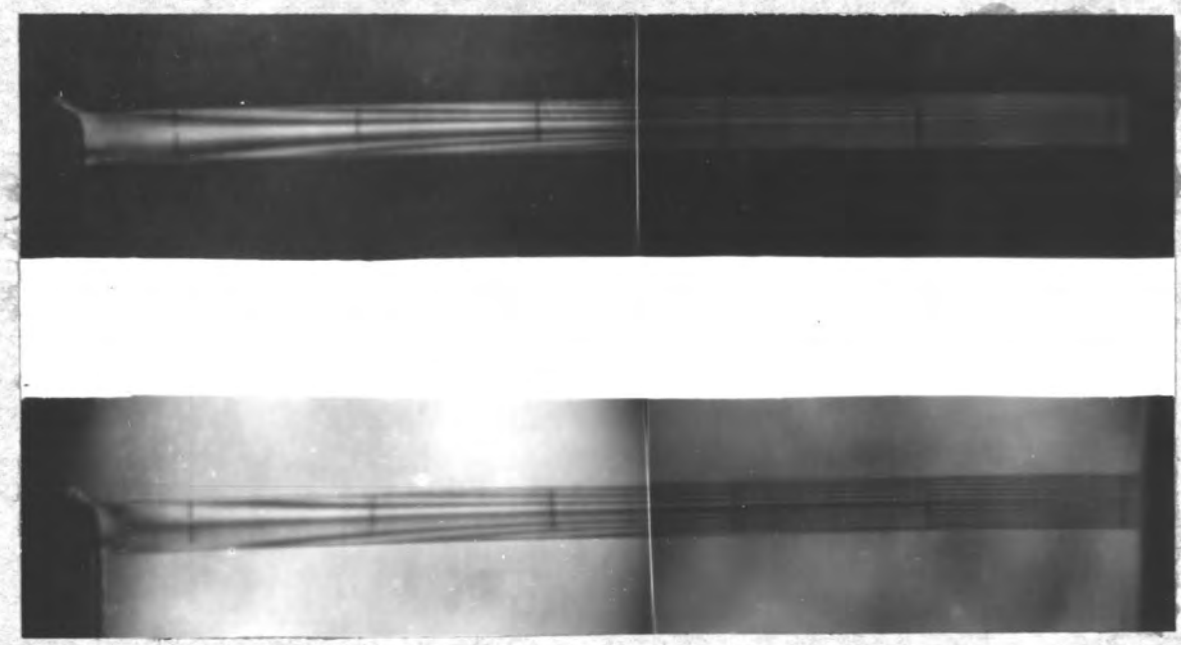

Figure 19. Stress patterns of a pinned end beam (Model No. 4) vibrating at the lowest resonant frequency photographed at point of maximum deflection. $y_m = 0.22$ in., $f = 62$ cycle/sec, $a = 0.20$ in.

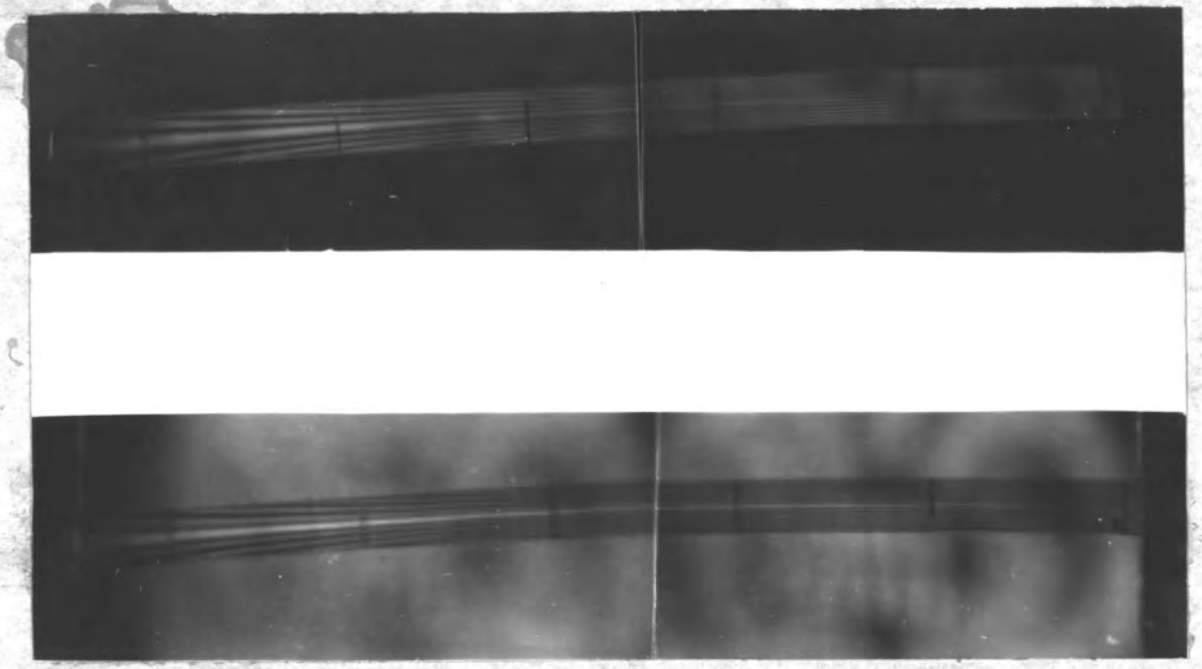

Figure 20. Stress patterns of a pinned end beam (Model No. 4) vibrating at the lowest resonant frequency photographed at the point of maximum deflection. $y_m = 0.32$ in., $f = 62$ cycle/sec, $a = 0.30$ in.

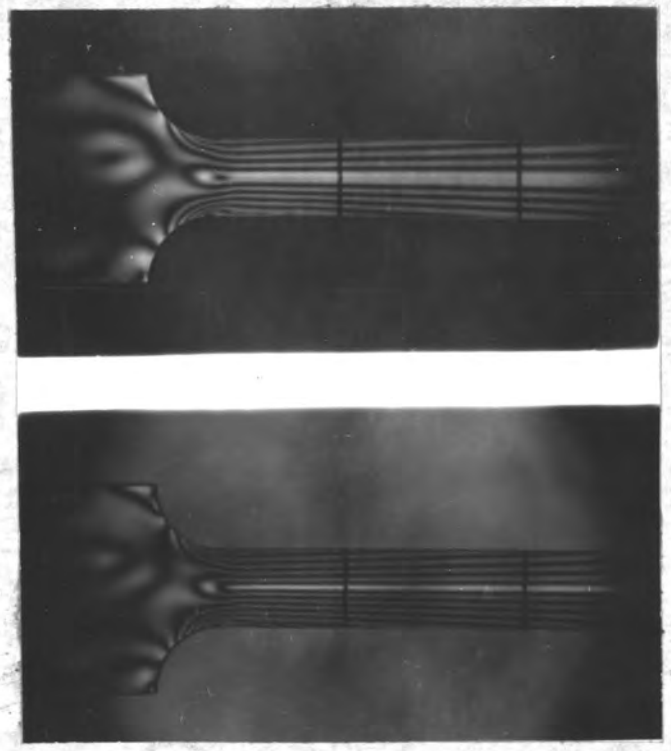

Figure 21. Stress pattern at the clamped end of a cantilever beam (Model No. 2) during resonant vibration for a fillet radius of 3/8 in. $y_m = 0.30$ in., f = 50 cycle/sec.

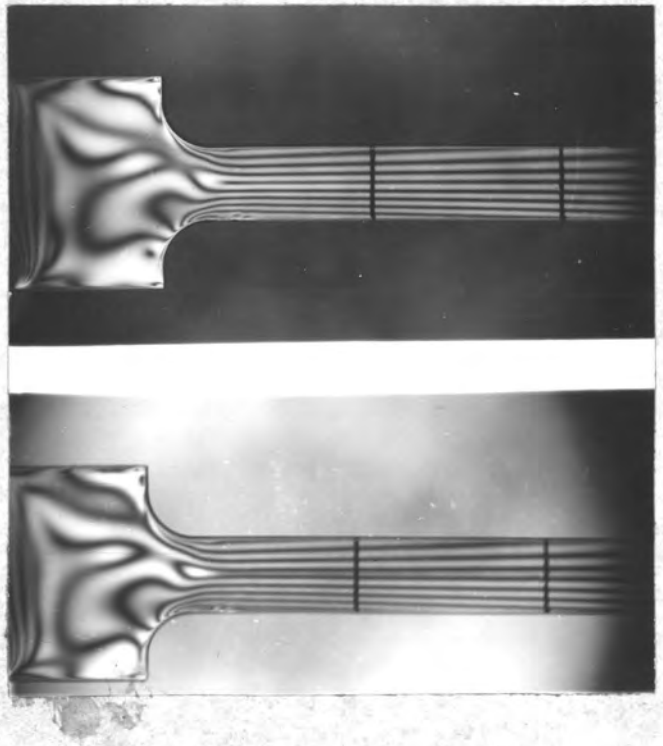

Figure 22. Stress pattern at the clamped end of a cantilever beam (Model No. 2) during resonant vibration for a fillet radius of 1/4 in. $y_m = 0.30$ in., f = 46 cycle/sec.

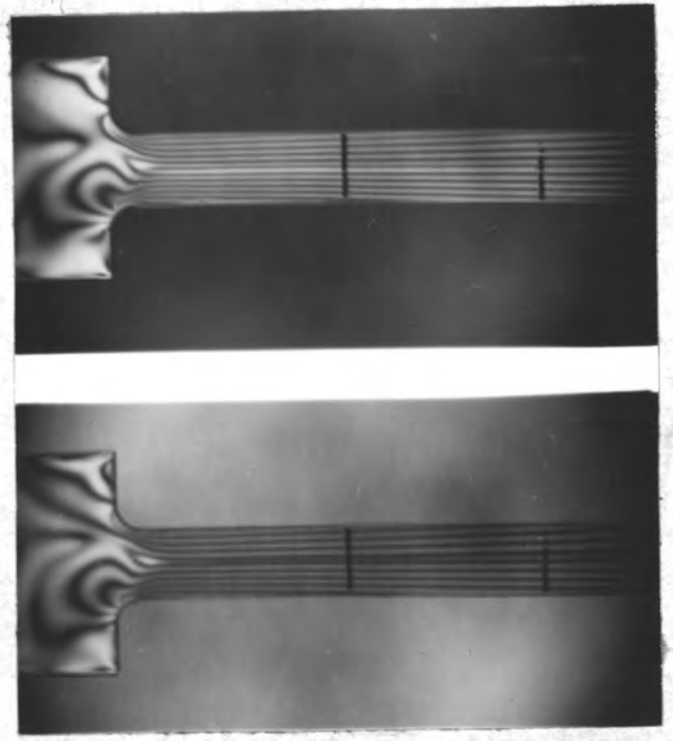

Figure 23. Stress pattern at the clamped end of a cantilever beam (Model No. 2) during resonant vibration for a fillet radius of 1/8 in.
$y_m = 0.30$ in., F = 40 cycle/sec.

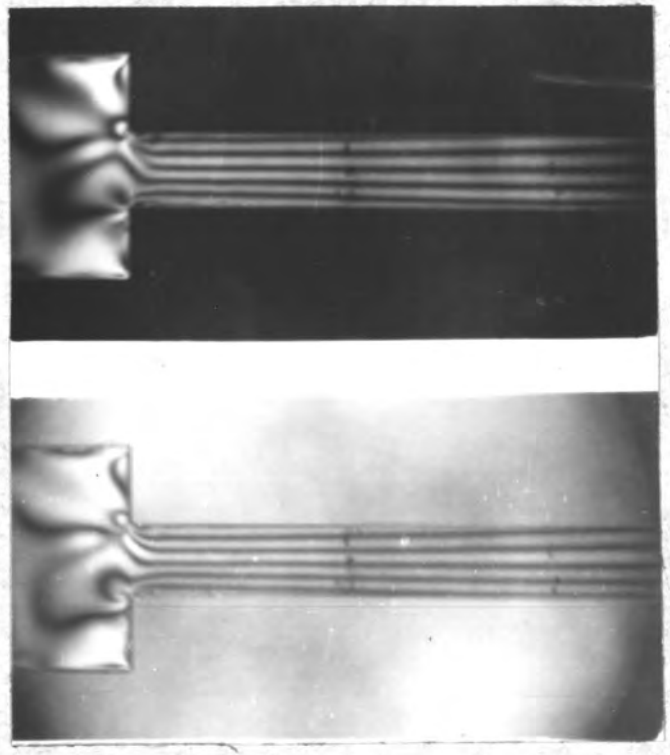

Figure 24. Stress pattern at the clamped end of a cantilever beam (Model No. 2) during resonant vibration for a fillet radius of zero. (square shoulder)
$y_m = 0.15$ in., f = 39.5 cycle/sec.

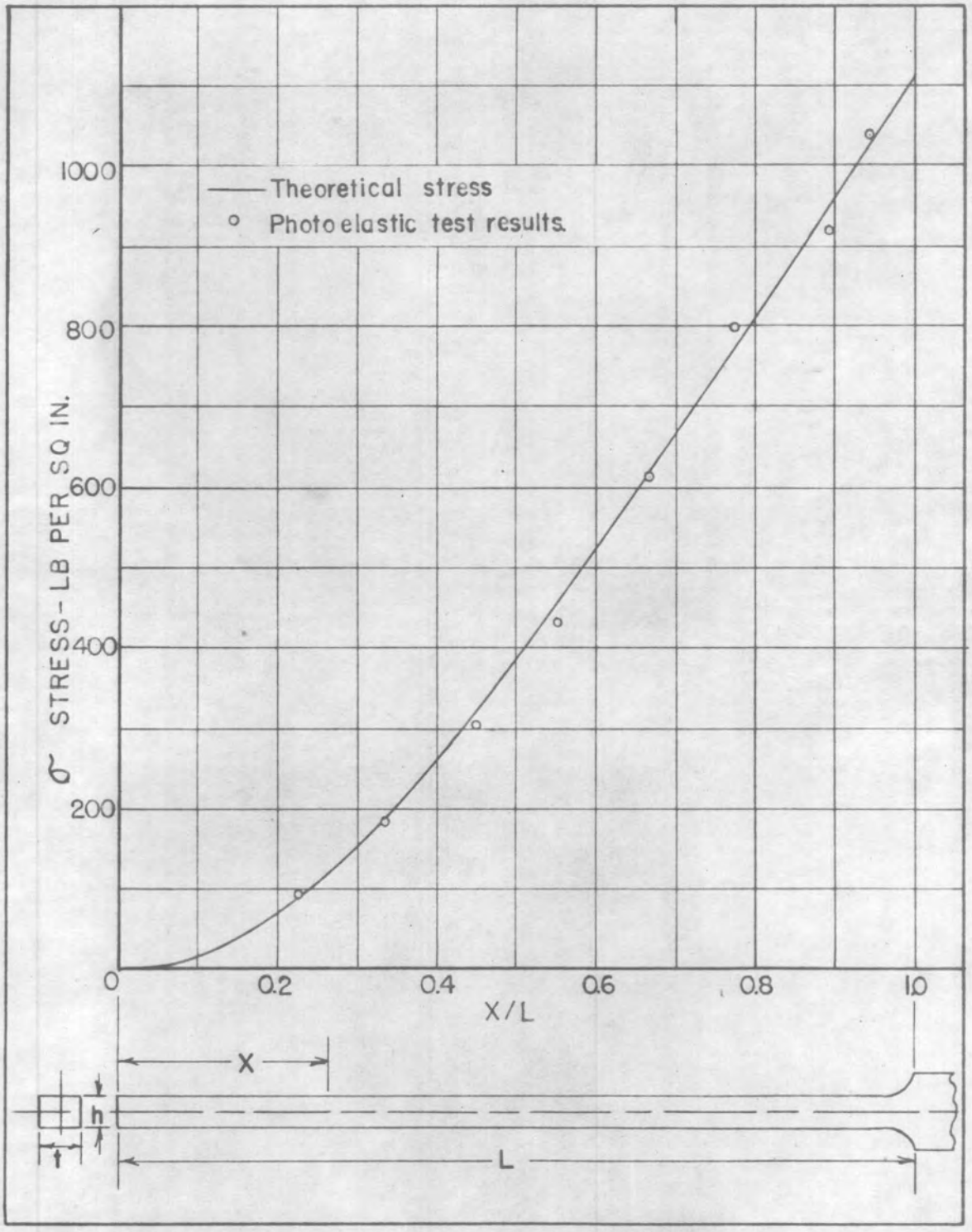

FIGURE 25. STRESS DISTRIBUTION AT THE OUTER FIBERS OF A CANTILEVER BEAM (MODEL NO.1) VIBRATING AT THE LOWEST RESONANT FREQUENCY. L = 9 IN., h = 0.375 IN., t = 0.340 IN., f = 55 CPS, Y_{max} = 0.25 IN.

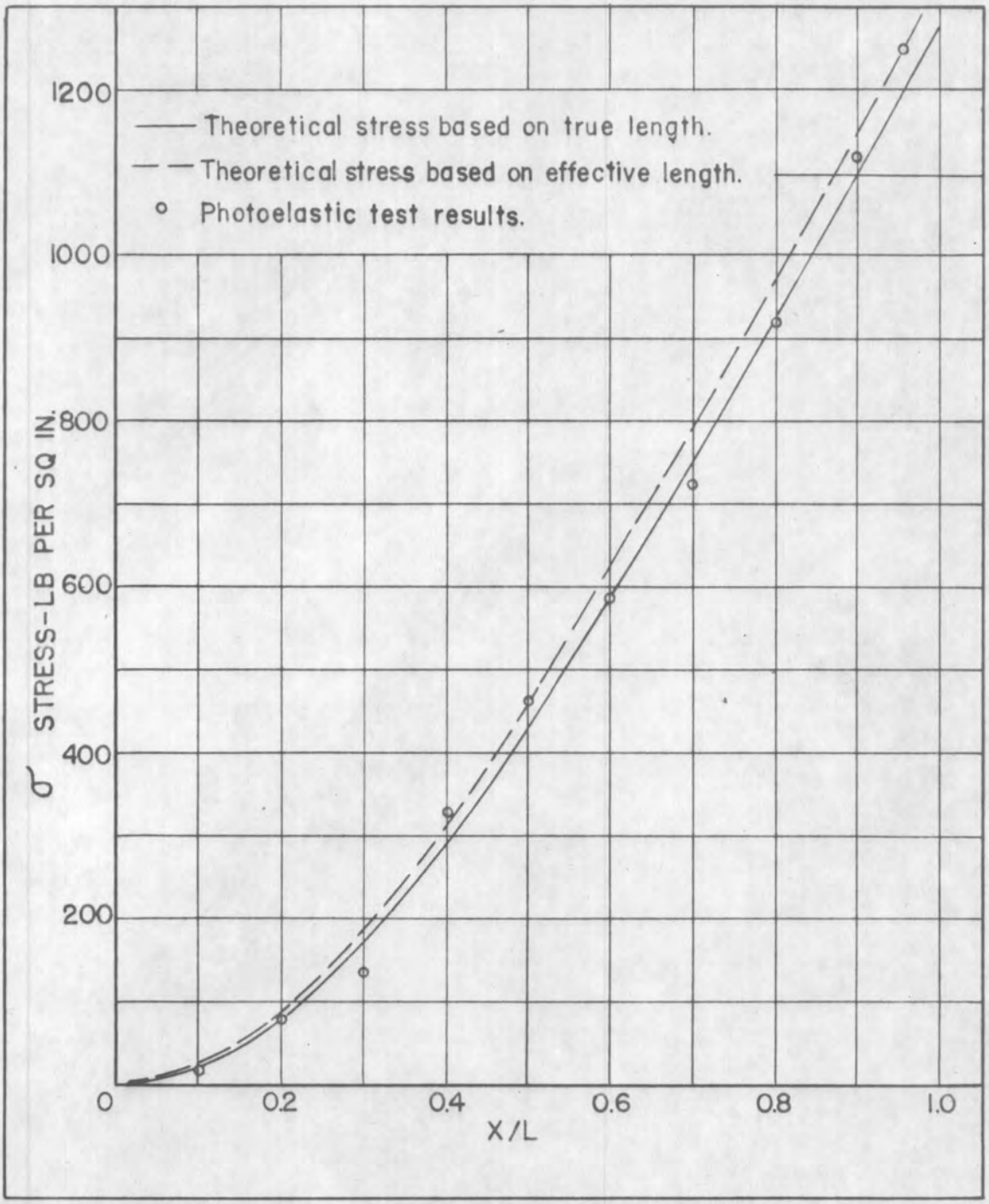

FIGURE 26. STRESS DISTRIBUTION AT THE OUTER FIBERS OF A CANTILEVER BEAM (MODEL NO. 2) VIBRATING AT THE LOWEST RESONANT FREQUENCY.
L = 10 IN., h = 0.430 IN., t = 0.317 IN., f = 50 CYCLE/SEC, Y_m = 0.3 IN.

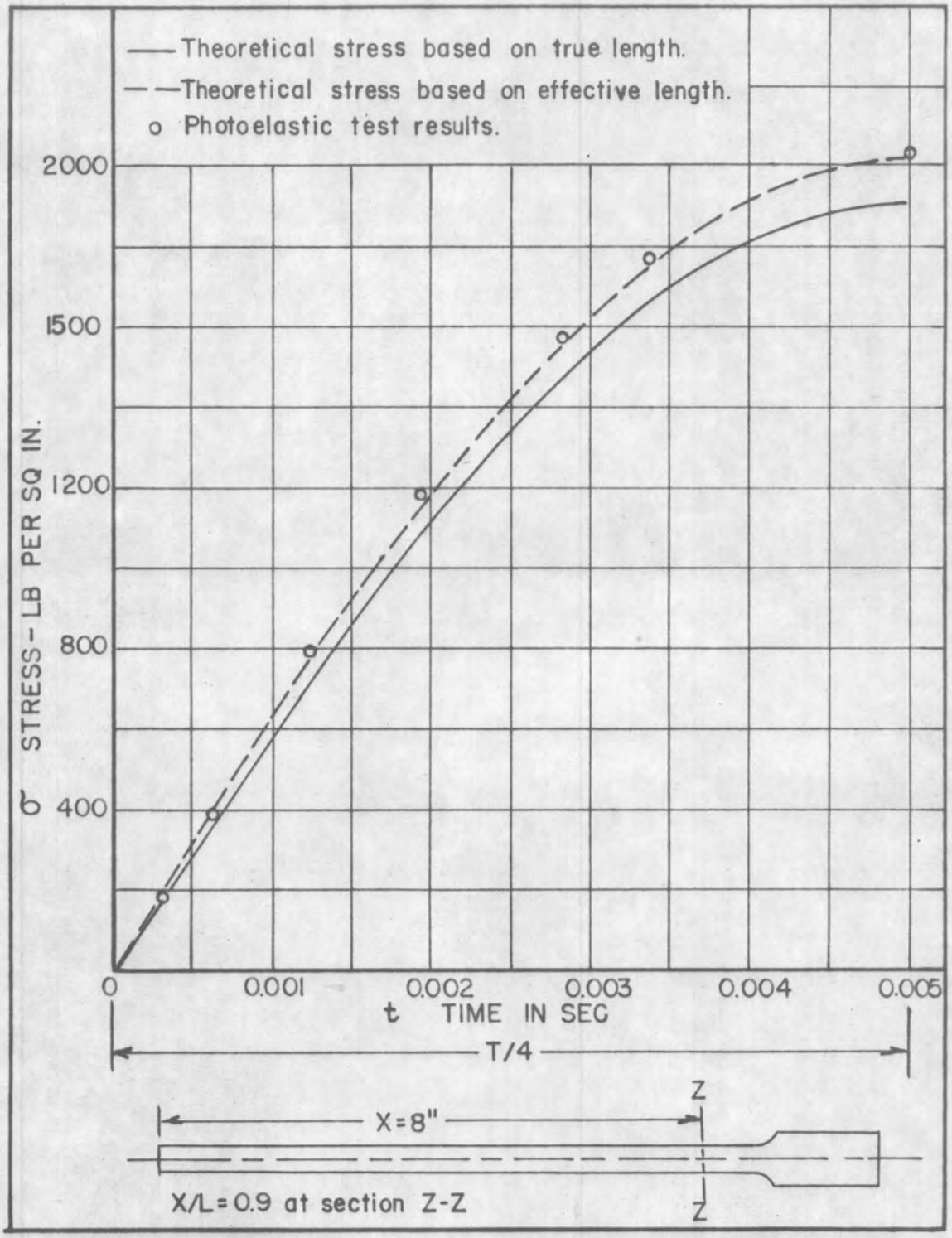

FIGURE 27. STRESS VARIATION AT THE OUTER FIBERS OF SECTION Z-Z ON A CANTILEVER BEAM (MODEL NO. 2) DURING ONE QUARTER OF A CYCLE OF RESONANT VIBRATION. T = 0.02 SEC, L = 10 IN., h = 0.430 IN., t = 0.317 IN., f = 50 CYCLE/SEC, Y_m = 0.52 IN.

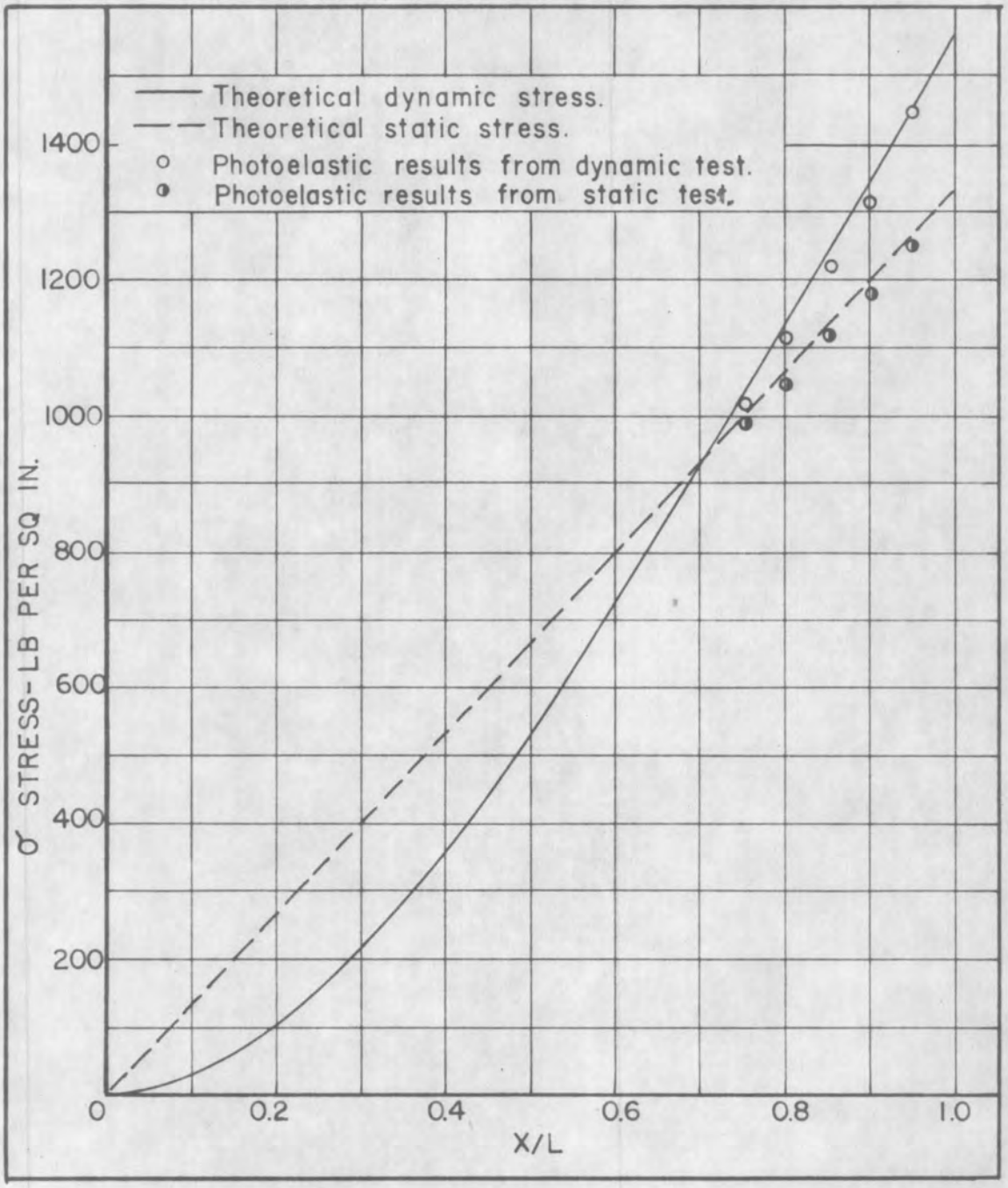

FIGURE 28. COMPARISON OF THE STRESS DISTRIBUTION AT THE OUTER FIBER OF A CANTILEVER BEAM (MODEL NO.2) DEFLECTED BY RESONANT VIBRATION AND BY STATIC LOADING. L = 10 IN., h = 0.404 IN., t = 0.317 IN., f = 46 CYCLE/SEC, Y_m = 0.40 IN.

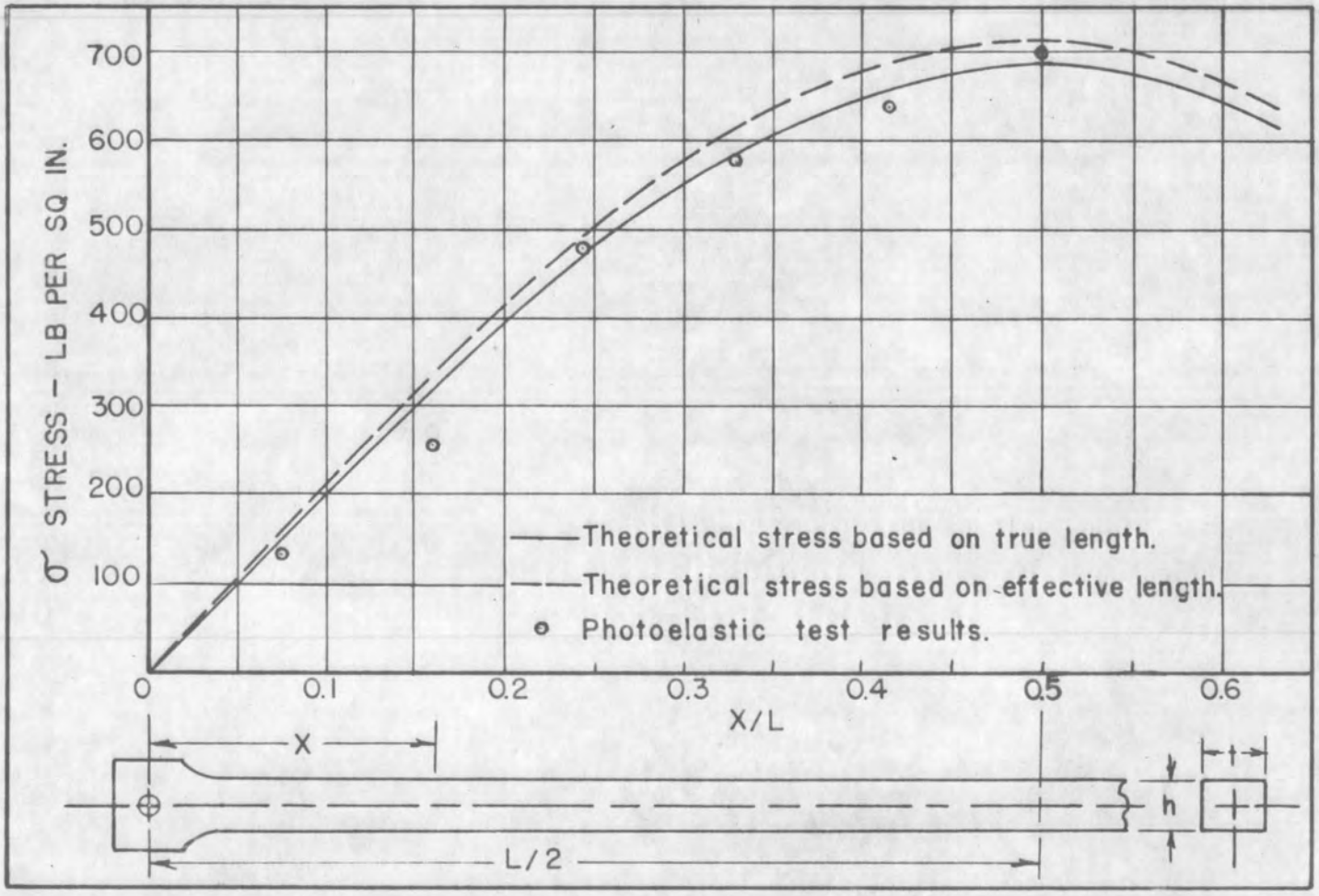

FIGURE 29. STRESS DISTRIBUTION AT THE OUTER FIBERS OF A PINNED END BEAM (MODEL NO. 3) VIBRATING AT THE LOWEST RESONANT FREQUENCY.
L = 11.75 IN., h = 0.250 IN., t = 0.327 IN., f = 57.5 CYCLE / SEC, Y_m = 0.14 IN.

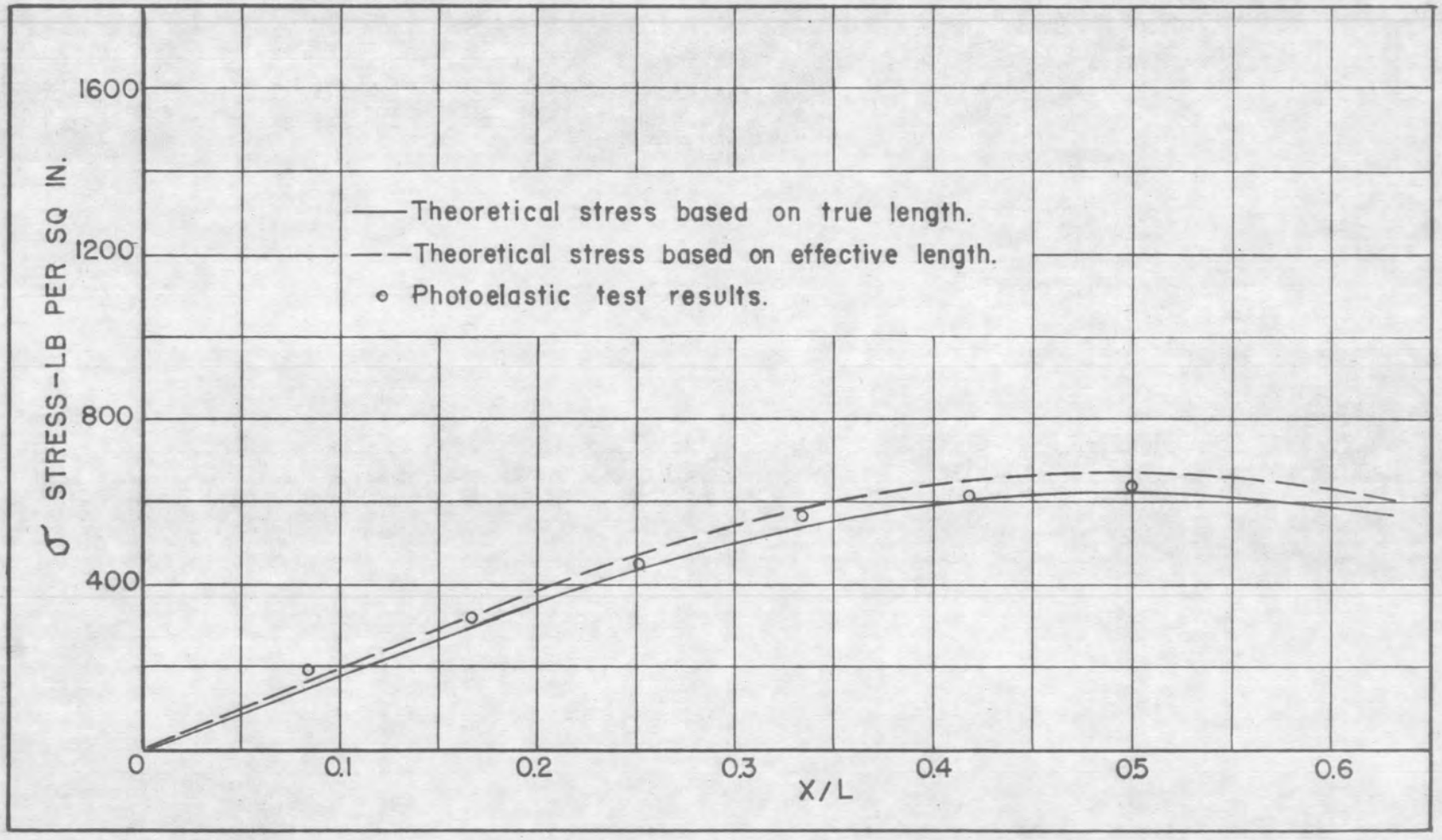

FIGURE 30. STRESS DISTRIBUTION AT THE OUTER FIBERS OF A PINNED END BEAM (MODEL NO. 4) VIBRATING AT THE LOWEST RESONANT FREQUENCY.
L = 12 IN., h = 0.275 IN., t = 0.325 IN., f = 62 CYCLE / SEC, Y_m = 0.12 IN.

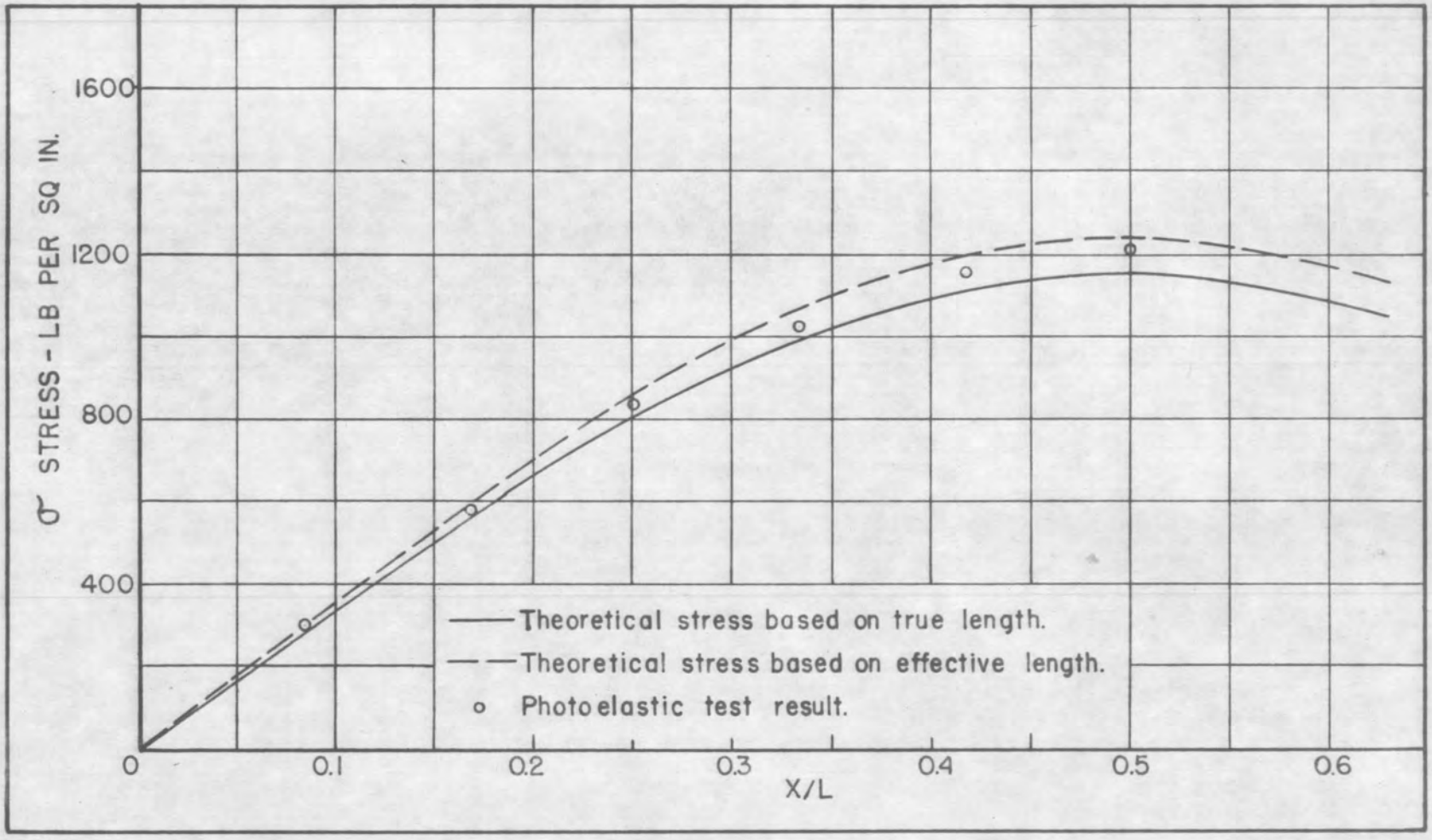

FIGURE 31. STRESS DISTRIBUTION AT THE OUTER FIBERS OF A PINNED END BEAM (MODEL NO. 4) VIBRATING AT THE LOWEST RESONANT FREQUENCY.
L = 12 IN. , h = 0.275 IN. , t = 0.325 IN. , f = 62 CYCLE / SEC , Y_m = 0.22 IN.

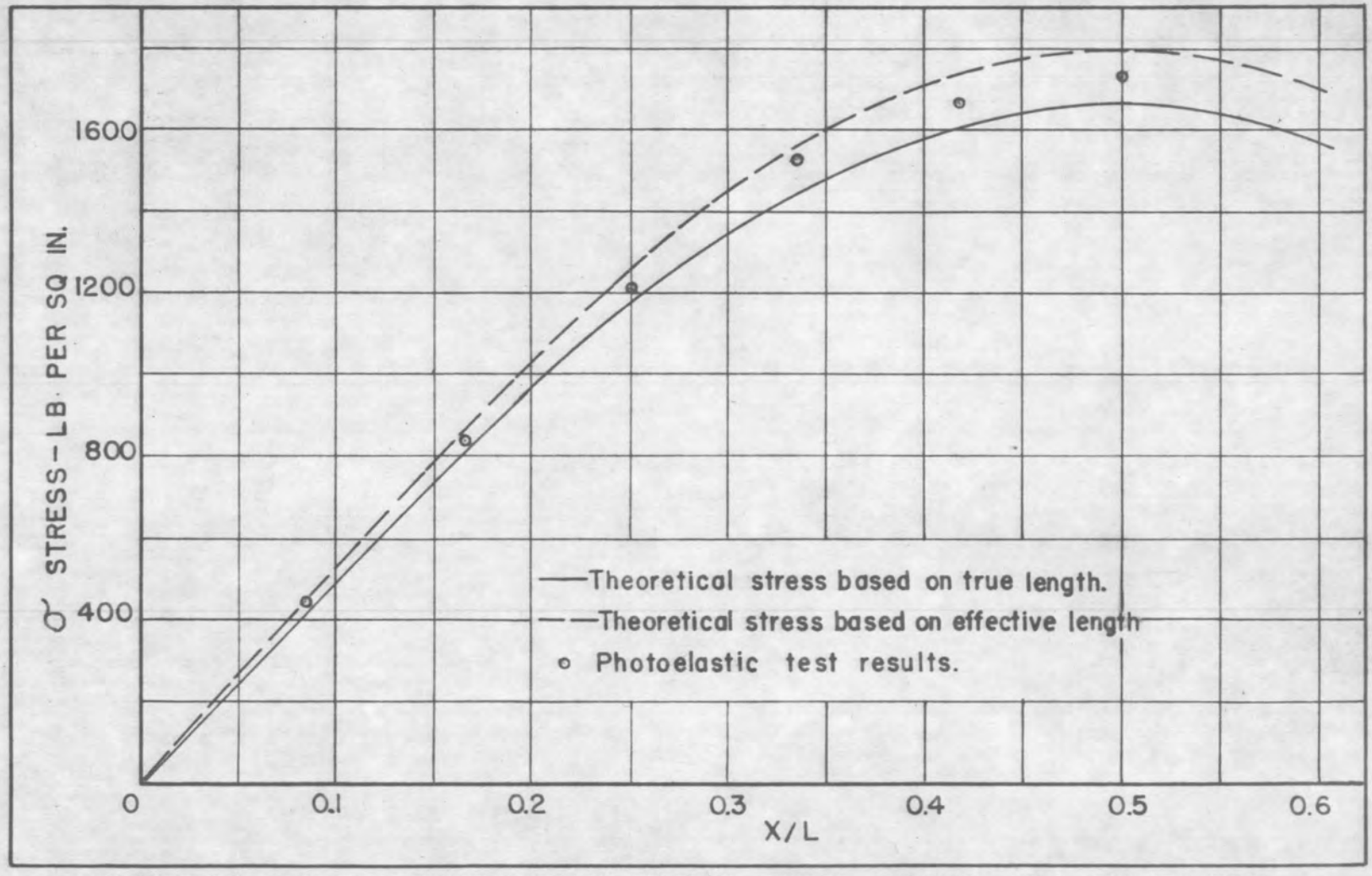

FIGURE 32. STRESS DISTRIBUTION AT THE OUTER FIBERS OF A PINNED END BEAM (MODEL NO. 4) VIBRATING AT THE LOWEST RESONANT FREQUENCY.
L = 12 IN., h = 0.275 IN., t = 0.325 IN., f = 62 CYCLE/SEC, Y_m = 0.32 IN.

DISCUSSION OF RESULTS

The photoelastic stress patterns induced in the beam models by resonant vibration are shown in Figures 10 through 24. The results obtained from these stress patterns are compared with the calculated theoretical results in Figures 25 through 32.

The theoretical stress distribution at the outer fibers of the cantilever beam models was calculated from equation (21). In Figures 26 and 27 two theoretical curves are shown. The second curve, indicated by a broken line, was calculated from equation (21) using the effective length given by equation (36). In the case of model no. 1, the true length and the effective length were approximately equal and only one curve was drawn. The effective length of model no. 2 was slightly less than the true or measured length, since the length was measured from the shoulder of the fillet and included a section of increased depth.

The stress distribution at the outer fibers of models no. 1 and 2 is shown in Figures 25 and 26. The test results were determined from Figures 10 and 12 with the aid of equation (44) of Appendix I. The fringe order at the tension and compression boundaries of the model was averaged to determine the value of n used in equation (44).

The sinusoidal vibration of stress with time at a point on the outer fibers of model 2 is shown in Figure 27. The test results were obtained from the stress patterns of Figures 13 through 15, which were photographed at various times during one quarter of a cycle of resonant vibration.

A comparison of the stress distribution induced at the outer fibers of model no. 2 by resonant vibration and by static loading is shown in Figure 28. In both cases, the maximum deflection at the free end of the beam was 0.40 of an inch. These curves indicate that the maximum stress induced in a cantilever beam by resonant vibration is slightly higher than that produced by a static load at the free end, causing the same maximum deflection. In both cases, the experimental and theoretical results are in agreement.

The theoretical stress distribution at the outer fibers of the pinned end beam models was calculated from equation (32) and the effective lengths were determined from equation (36). The effective length of both models was slightly less than the measured length. This can be partially attributed to the inertia effects of the portion of the beam projecting beyond the pin supports and the increased cross-section at the ends.

The photoelastic test results, obtained from the

stress patterns of the pinned end beam models, is compared with the theoretical stress distribution at the outer fibers of Figures 29 through 32. These curves show that the stress at the outer fibers of a pinned end beam, vibrating in the first mode, varies sinusoidally between the supports and has a maximum value at the center.

The stress patterns of Figures 21 through 24 were photographed in an attempt to determine the effect of fillet radius on the stress concentration induced in a cantilever beam by resonant vibration. No quantitative results were obtained from these photographs because of the indistinctness of the fringes at the fillets of small radius. No sizeable stress concentration was indicated at the fillets of 3/8, 1/4, or 1/8 inch radius, however, there is indication of considerable stress concentration in the case of the square shoulder.

The experimental and theoretical results agreed within 5 percent, in all cases, except at points of very low stress, such as existed at the free end of the cantilever beam models.

CONCLUSIONS

The excellent agreement between the experimental and theoretical results indicates that the polariscope employed in this investigation is suitable for the photoelastic analysis of models subjected to steady state vibration and impact.

The experimental results were obtained using the static value of the fringe constant. It can, therefore, be concluded that the static and dynamic values of the fringe constant are approximately equal or equal and that frequency and acceleration have no appreciable effect on the photoelastic properties of S-4 48306 Bakelite. This statement may not be true for extremely high frequencies or rates of loading.

The light source employed in this investigation is not satisfactory for the study of transient stresses. A consideration of the speed, with which transient stress patterns change, indicates that a light source, with a flash duration of the order of 1/10 microsecond, is required to successfully photograph transient stress patterns.

The addition of a diffuser to the polariscope would increase the field size and simplify the analysis of large photoelastic models.

A polariscope of the type employed in this investigation would be ideal for static photoelastic work where special methods of loading are required. The short flash duration eliminates the necessity of a heavy rigid frame and makes the units easily portable.

BIBLIOGRAPHY

1. Baruch, J. J. The design of high speed polariscope. Proceedings of the society for experimental stress analysis, vol. 8, no. 1: pp. 197-204. 1950.

2. Charlton, T. M. Recent experimental methods. North-east coast institute of engineers and ships transactions, vol. 65; pp. 28-46. Nov. 1948.

3. Crawford, A. E. Electronic stroboscope. Aircraft productions, vol. 10, no. 113: pp. 101-102. Mar. 1948.

4. Findley, W. N. The fundamentals of photoelastic stress analysis applied to dynamic stresses. Proceedings of ninth semi-annual eastern photo-elastic conference. pp. 1-13. May 1939.

5. Foeppl, Ludwig. Slow motion pictures of impact tests by measns of photoelasticity. Journal of applied mechanics, vol. 16, no. 2: p. 173. June 1949.

6. Frocht, Max M. Kinematography in photoelasticity. Transactions of american society of mechanical engineers, APM 54-9: p. 83. 1932.

7. Frocht, Max M. Photoelasticity. vol. 1, New York, Wiley, 1941, 411 p.

8. von Karman, Theodore and M. A. Biot. Mathematical methods in engineering. New York, Mc Graw, 1940. 439 p.

9. Kirmser, P. G. The effect of discontinuities on the natural frequency of beams. Proceedings of the american society of testing materials, vol. 44: p. 897. 1944.

10. Murray, W. M. Photoelastic study in vibrations. Journal of applied physics, vol. 12, no. 8: pp. 617-622. Aug. 1941.

11. Stanton, J. S. A method of assessing transient stresses in photoelastic substances. Review of scientific instruments, vol. 20, p. 139. Feb. 1949.

12. Thomson, W. T. Vibration of slender bars with discontinuities in stiffness. Journal of applied mechanics, vol. 16, no. 2: p. 203 June 1949.

13. Timoshenko, Stephen. Strength of materials, part 2, New York, Van Nostrand, 1940. 510 p.

14. Timoshenko, Stephen. Vibration problems in engineering. 2 ed. New York, Van Nostrand, 1937. 470 p.

15. Tuzi, Z. and M. Nisida. Photoelastic study of stresses due to impact. Philosophic magazine. S7 vol. 21, no. 140, supplement. pp. 448-473. Feb. 1936.

16. Wyle, F. S. Some photoelastic studies in dynamics. Proceedings of thirteenth semi-annual photoelastic conference. pp. 13-18. 1941.

APPENDIX I

DETERMINATION OF THE FRINGE CONSTANT

In order to obtain quantitative results from photoelastic tests, the fringe constant for the material is required.

A beam in pure bending was used to determine the fringe constant of S-4 48306 Bakelite. The dimensions of the model and the method of loading is shown in Figure 33.

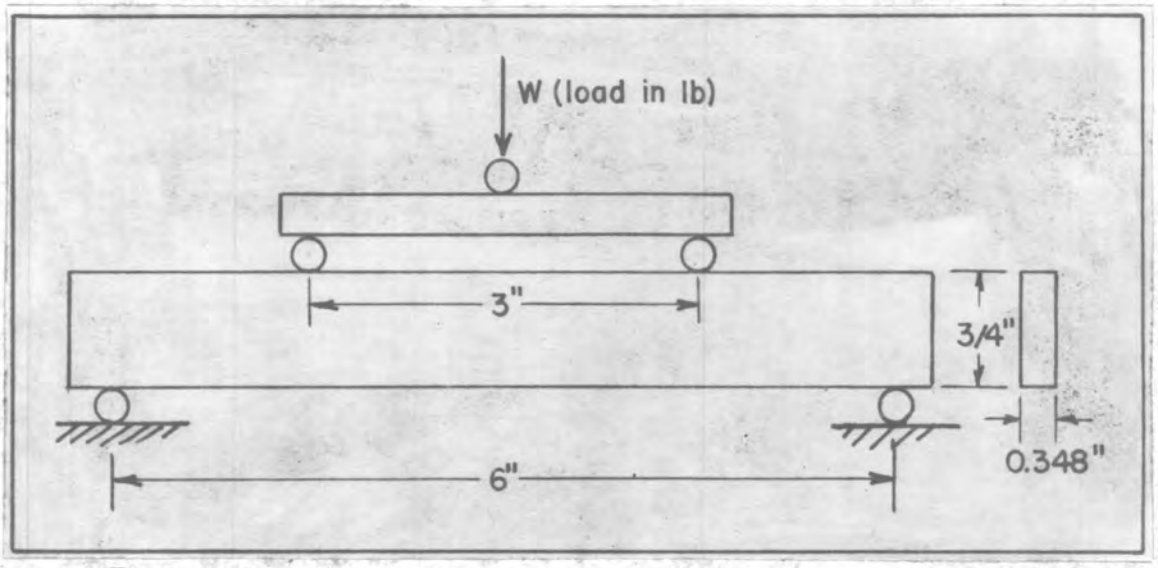

Figure 33. Calibration model for determining the fringe constant of S-4 48306 Bakelite.

The relationship between the fringe order and the difference between the principal stresses is

$$p - q = f\left(\frac{n}{t}\right) \qquad (41)$$

where f is the fringe constant. By rearranging equation (41), the following relation is obtained from which the

fringe constant can be determined.

$$f = (p-q)\frac{t}{n} \tag{42}$$

At the outer fibers of an unloaded portion of a beam $q = 0$ and the stress p is given by the equation,

$$p = \frac{Mh}{2I} = \frac{6M}{th^2}.$$

Substituting this value in equation (41),

$$f = \frac{6M}{nh^2}.$$

Substituting $M = 3/4W$ and $h = 3/4$ in. from Figure 33,

$$f = 8\left(\frac{W}{n}\right).$$

The value of (W/n) was determined by counting the number of fringes on the model at load increments of 25 pounds. The fringe patterns photographed at loads of 75 and 100 pounds are shown in Figure 34 and 35. The curve plotted from this data is shown in Figure 36.

Substituting the value of (W/n) from Figure 36, the value of the fringe constant is

$$f = 8(10.43) = 83.4. \tag{43}$$

Knowing the fringe constant, the difference of the principal stresses is given by the equation,

$$p-q = 83.4\frac{n}{t}. \tag{44}$$

Equation (44) is valid only when the polariscope utilizes the 4800 Angstrom unit band of light and the photoelastic material is S-4 48306 Bakelite.

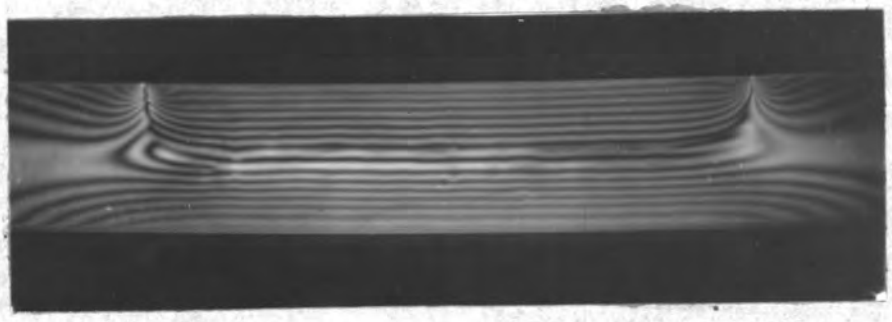

Figure 34. Calibration test of a S-4 48306 Bakelite beam in pure bending. W = 75 lb.

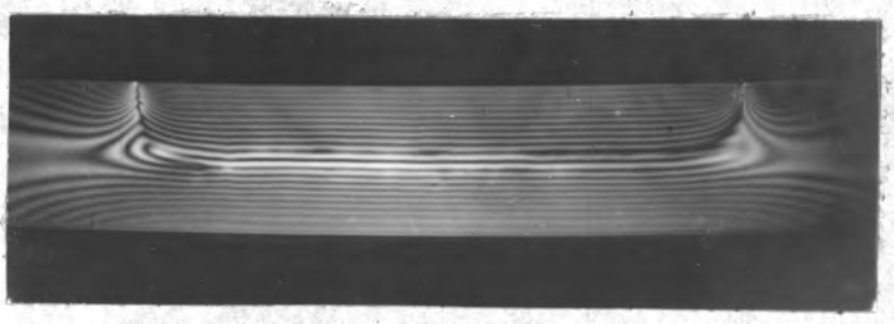

Figure 35. Calibration test of a S-4 48306 Bakelite beam in pure bending. W = 100 lb.

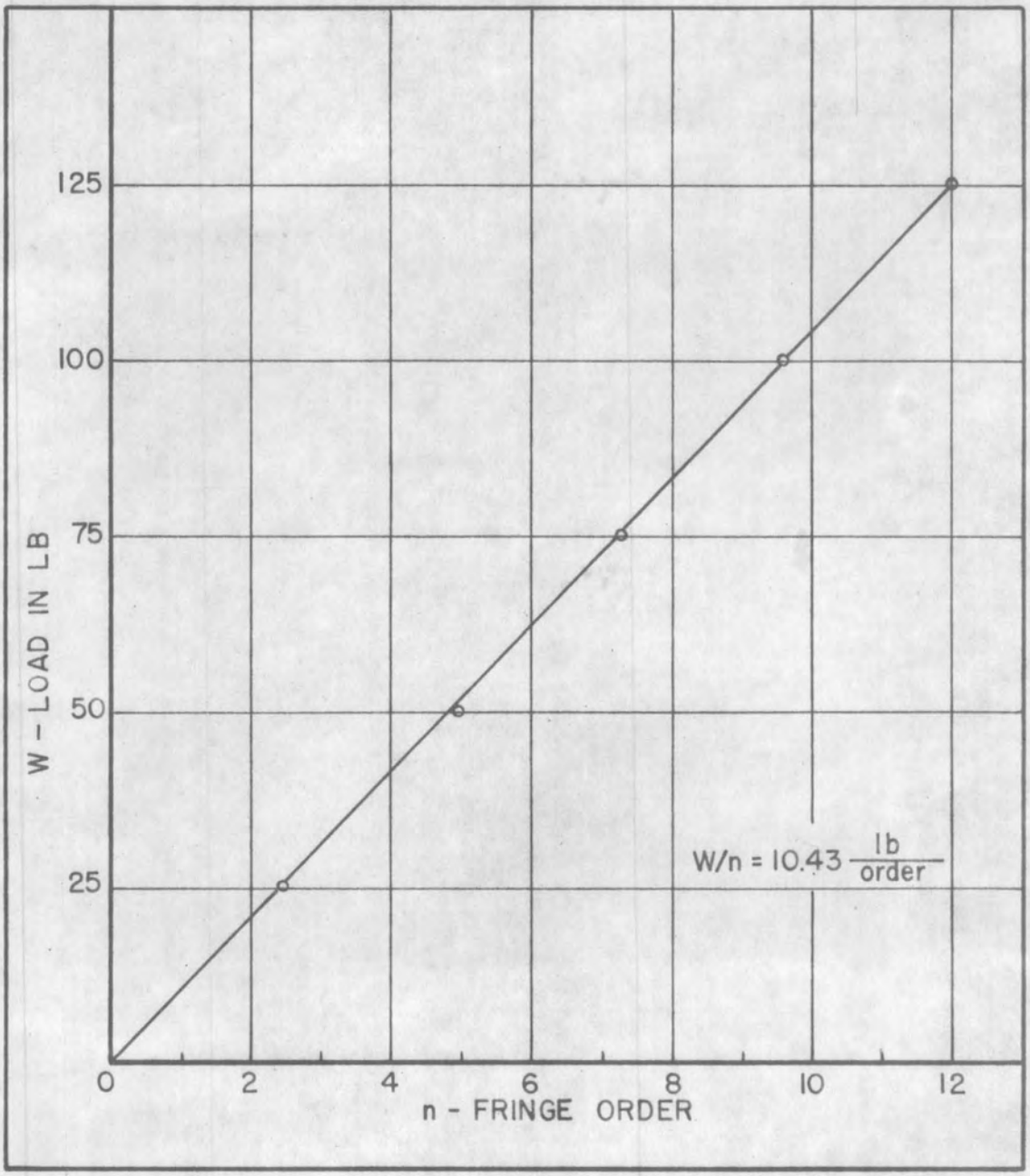

FIGURE 36 VARIATION OF FRINGE ORDER WITH LOAD ON A S-4 48306 BAKELITE BEAM IN PURE BENDING.

APPENDIX II

DETERMINING THE MODULUS OF ELASTICITY OF S-4 48306 BAKELITE.

The physical properties of Bakelite vary quite widely, depending upon the manner of annealing, age, temperature, humidity and storage conditions.

A tension specimen was cut from each sheet of Bakelite used during the investigation. Tension loads were applied to the specimen using the loading frame of the photoelastic bench. Strain readings were taken with two Huggenberger Tensomenters at load increments of 25 pounds.

Failure of both specimens occurred at the pin supports before the yield point of the material was reached.

The modulus of elasticity for the two specimens was as follows:

Specimen No. 1 (sheet no. 1) E = 550,000 lb/sq in.

Specimen No. 2 (sheet no. 2) E = 558,000 lb/sq in.

The stress-strain diagram obtained from the test of specimen No. 2 is shown in Figure 37.

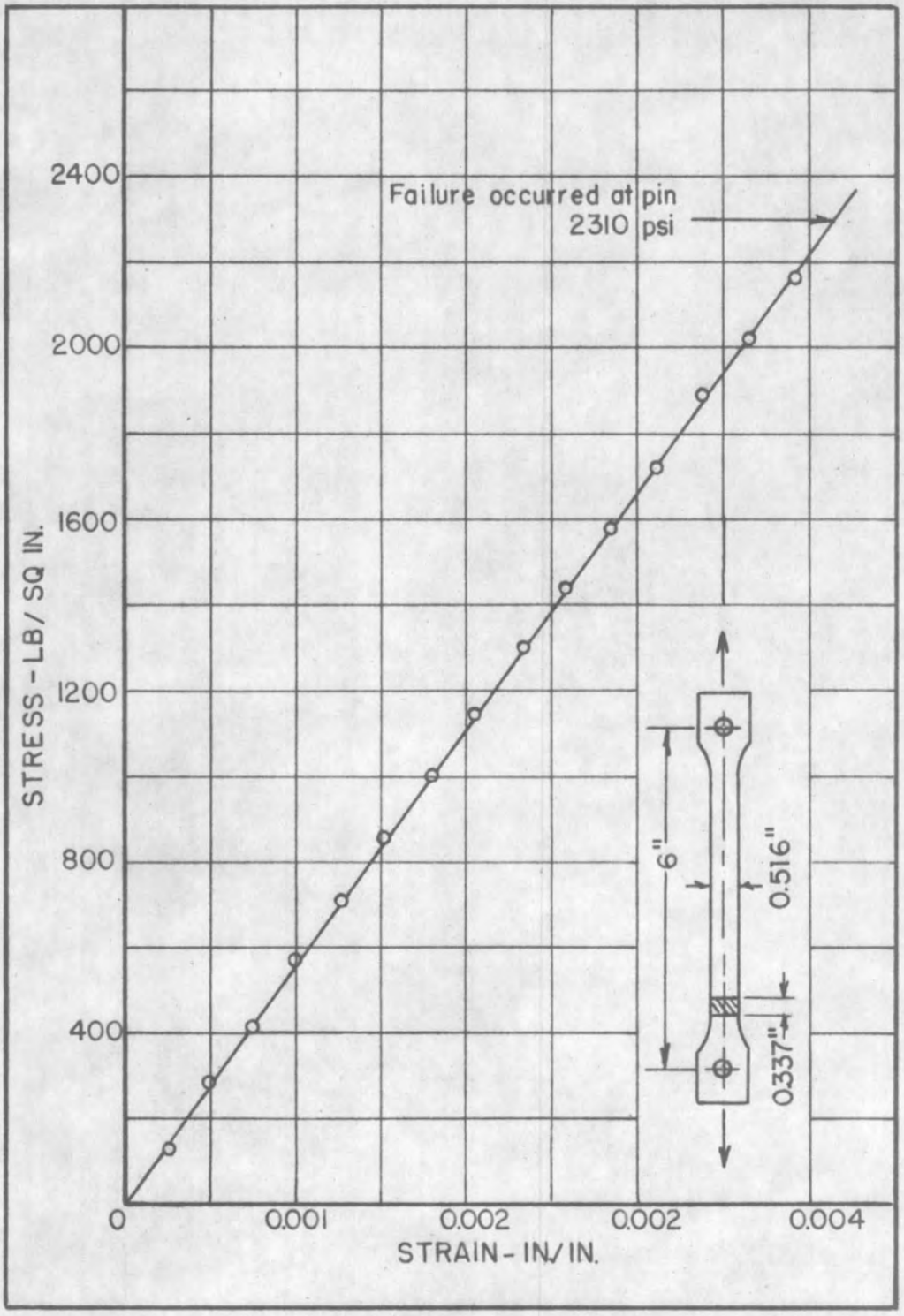

FIGURE 37 STRESS STRAIN DIAGRAM
FOR BAKELITE S-4 48306 IN TENSION.